

The Chemical Evolution of Galaxies

Mirko Curti^a

^aEuropean Southern Observatory, Karl-Schwarzschild-Strasse 2, 85748 Garching, Germany

© 20xx Elsevier Ltd. All rights reserved.

Nomenclature

4MOST	4-metre Multi-Object Spectroscopic Telescope
ADF	Abundance Discrepancy Factor
AGN	Active galactic nucleus
APOGEE	APO Galactic Evolution Experiment
BPT	Baldwin–Phillips–Terlevich
CC-SNe	Core-collapse supernovae
CEL	Collisionally-excited lines
CEMP	Carbon-enhanced metal-poor stars
CGM	Circumgalactic medium
DLA	Damped Lyman- α system
E-ELT	European extremely large telescope
ESO	European Southern Observatory
EW	Equivalent width
FMR	Fundamental metallicity relation
ICM	Intracluster medium
IFU	Integral field unit
IFS	Integral field spectroscopy
IGM	Intergalactic medium
IMF	Initial mass function
IR	Infrared
ISM	Interstellar medium
JWST	James Webb Space Telescope
LLS	Lyman Limit System
MaNGA	Mapping nearby galaxies at APO
MOONS	Multi object optical and near-infrared spectrograph
MUSE	Multi unit spectroscopic explorer
MW	Milky Way
MZR	Mass–metallicity relation
RL	Recombination lines
SAMI	Sydney-AAO Multi-object Integral field spectrograph
SDSS	Sloan digital sky survey
SFR	Star formation rate
SSP	Single stellar population
UV	Ultraviolet
VLT	Very large telescope

Abstract

Metals—heavy elements synthesized during various phases of stellar evolution or during supernova explosions—play a fundamental role in shaping galaxy evolution. In fact, their relative abundances, spatial distribution, and scaling with galactic properties reflect the constant interplay between star-formation, nucleosynthesis, and gas flows that drive the cycle of baryons in-and-out of galaxies across the cosmic time. This chapter aims at offering a concise introduction to the methodologies used to measure elemental abundances in galaxies and the basics of chemical evolution modeling. We also provide a brief overview of the current observational framework, including metallicity scaling relations, the study of relative chemical abundances, the distribution of metals within and beyond galaxies, and how these properties evolve with redshift, drawing on both extensive literature and recent developments, and aiming to highlight well-established findings alongside ongoing challenges in this rapidly advancing field.

Keywords

Galaxies:Emission line galaxies; Galaxies:High-redshift galaxies; Galaxy physics:Galaxy formation; Galaxy physics: Galaxy abundances; Chemical Abundances:Metallicity; Chemical Abundances:Abundance ratios

Key points

- **Metallicity** The abundance of all elements heavier than hydrogen and helium relative to the total mass of baryons. Often expressed in terms of relative number densities.
- **Oxygen abundance** The relative abundance of oxygen compared to hydrogen. It is often adopted as a proxy for the total metallicity of a galaxy.
- **Stellar metallicity** The mass-weighted or luminosity-weighted metallicity of stellar populations. It reflects the integrated star-formation history of a galaxy.
- **Gas-phase metallicity** The metallicity of the gas-phase of the ISM, reflecting the ‘current’ level of chemical enrichment and probing recent star-formation episodes and short-timescales processes and gas flows.
- **Te-method** A methodology to derive gas-phase abundances from the direct measurement of the temperature of free electrons in the ionized gas
- **Strong-line methods** Ratios of bright emission lines in galaxy spectra calibrated as gas-phase metallicity diagnostics
- **Absorption line system** A gas cloud observed against a background source of radiation, producing absorption lines in the spectrum whose properties depend on the intervening column density
- **Damped Lyman alpha** Absorption system with column density $N_{\text{HI}} > 10^{20.3} \text{ cm}^{-2}$
- **Closed-box model** Analytical chemical evolution model assuming no gas flows in-and-out of the system
- **Stellar yield** The amount of metals produced by a stellar generation and returned to the ISM
- **Effective yield** The effective (lower) value of the stellar yield that account for metals expelled within gas outflows
- **Mass-Metallicity relation** The scaling relation between the stellar mass content and the metallicity (either stellar or gas-phase) observed in galaxy populations.
- **Fundamental metallicity relation** The scaling relation between stellar mass, metallicity, and star-formation rate. Galaxies with high SFR have on average lower metallicity than low-SFR systems for the same stellar mass.
- **Chemical abundance patterns** Relative abundances of different elements. Their trends with total metallicity and cosmic time constrain the history of star-formation in galaxies.
- **Metallicity gradient** Trend of metal enrichment with galactocentric radius.
- **Metal budget** Accounting for the total amount of metals produced by galaxies by studying their distribution over different phases.

1 Introduction

In the Λ CDM cosmological framework, the Universe consists primarily of baryons, dark matter, and dark energy, which collectively influence the shape of space and the arrangement of cosmic structures. Structure formation is driven by gravity, which amplifies small irregularities in the dark matter’s otherwise uniform distribution. When these irregularities grow to a certain size, they form dark matter halos—gravitationally bound regions that continue to expand through matter accumulation and mergers with smaller structures. As gas cools within these halos, conditions emerge that enable star formation, leading to the first massive, metal-free (Population III) stars. These early stars quickly exhausted their fuel, producing the first metals that enriched the surrounding interstellar medium (ISM).

Once they have formed, galaxies continuously undergo chemical enrichment. Metals produced via stellar nucleosynthesis or during violent Supernovae explosions are then returned to the ISM, enriching the galactic environment. In addition, cosmological accretion from the cosmic web and outflows driven by either star-formation or super-massive black holes activity further regulate the metal content of the ISM. The continuous interplay among these processes drives the baryonic cycle in and out of galaxies, and shapes the scaling relations between metallicity and other global properties which are observed in galaxy populations in both the nearby Universe and at early cosmic epochs. Furthermore, different chemical species are produced (and returned to the ISM) on different timescales by stars of different masses; therefore, the relative abundance of elements provides unique and complementary insights on the star-formation history of galaxies. Overall, the analysis of the chemical properties of galaxies and their evolution with cosmic time deliver therefore key observational constraints that need to be matched by any model and simulation aimed at describing how galaxies form and evolve.

Throughout this Chapter, we will provide an overview on the chemical properties of galaxies in both the local and early Universe. We will first discuss the main techniques adopted to measure chemical abundances in stellar populations and in the interstellar medium of galaxies, addressing strengths and weaknesses of the different methods. Then, we will introduce some simple realizations of chemical evolution models, and discuss how the parameters in these models are directly linked to the physical processes driving the mass assembly, star-formation, and chemical enrichment in galaxies over cosmic time. Finally, we will present a brief overview of the current observational landscape of the field (including some of the most recent developments from the James Webb Space Telescope, JWST), focusing in particular on the metallicity scaling relations in galaxies and their evolution with redshift, the study of different chemical abundance patterns, and the distribution of metals inside and outside galaxies.

2 Metallicity measurements in galaxies

2.1 Some definitions

In the astrophysical context, the word ‘metals’ refers to all chemical elements heavier than hydrogen and helium. By strict definition, the ‘metallicity’ indicates the abundance by mass of all metals relative to the total mass of baryons (which is dominated by hydrogen and helium). However, in galaxy evolution studies the relative abundance of two elements is generally expressed in terms of their relative number densities, such that

$$X/Y \equiv N_X/N_Y. \quad (1)$$

When expressing the relative abundance of a given ionic species relative to hydrogen, the following notation is also commonly adopted

$$12 + \log(X/H) \equiv 12 + \log(N_X/N_H) \quad (2)$$

where the value 12 is added to ensure such expression provides always a positive value, or

$$[X/H] \equiv \log(N_X/N_H) - \log(N_X/N_H)_\odot \quad (3)$$

when expressing quantities relative to Solar abundances. Since measuring elemental abundances is often observationally challenging, in galaxy evolution studies it is common practice to assume the oxygen abundance ($12 + \log(O/H)$) as a proxy of the total metallicity, as oxygen is generally the most abundant heavy element by mass and it is responsible for the brightest emission lines seen in galaxy spectra (hence it is often the only element whose abundance can be reliably measured). This approximation assumes that the abundances of all other heavy elements scale proportionally to Solar abundance ratios which, as we will see later on, it might often be an incorrect assumption in early galaxies. Furthermore, the exact value of the Solar oxygen abundance can vary depending on the measurement techniques, in that for instance hydrodynamical models of the solar atmosphere provides a photospheric oxygen abundance of $12 + \log(O/H)_\odot = 8.69 \pm 0.05$ (Asplund et al., 2009), whereas studies based on helioseismology delivers higher values, i.e. $12 + \log(O/H)_\odot = 8.86 \pm 0.05$ (Delahaye and Pinsonneault, 2006). Nonetheless, in the framework of galaxy evolution studies the absolute Solar abundance values should only be considered as a reference, although care should be taken in rescaling observational results of chemical abundances in galaxies to the same Solar abundance scale when comparing different studies.

2.2 Stellar metallicity

The metallicity of the stellar populations provides information on the integrated star-formation history of galaxies, as it reflects the total amount of heavy elements built throughout subsequent stellar generations across galaxy lifetimes and currently locked into stars. Elemental abundances in the stellar photospheres are reflected into a wealth of characteristic absorption features observable in the continuum of galaxy spectra, and which have been extensively calibrated against models to identify robust stellar metallicity diagnostics.

2.2.1 Spectral absorption features and indices

Historically, early approaches involved the development of a set of spectral indices, including the so-called Lick indices, defined as the ratio of the flux measured within a given bandpass (typically $\sim 50\text{\AA}$ width) and that of a nearby pseudo-continuum evaluated in two nearby wavelength windows, such as (Worthey et al., 1994, following the definition of) :

$$\text{Index} = \int_{\lambda_1}^{\lambda_2} \left(1 - \frac{f_\lambda}{F_C} \right) d\lambda, \quad (4)$$

where f_λ is the observed flux density at wavelength λ , λ_1 and λ_2 are the boundaries of the feature bandpass, and with the pseudo-continuum F_C estimated as

$$F_C = \frac{\lambda_r - \lambda}{\lambda_r - \lambda_b} \cdot \langle f_\lambda \rangle_{\lambda_b} + \frac{\lambda - \lambda_b}{\lambda_r - \lambda_b} \cdot \langle f_\lambda \rangle_{\lambda_r}, \quad (5)$$

where $\langle f_\lambda \rangle_{\lambda_b}$ is the average flux density in the blue pseudo-continuum bandpass, $\langle f_\lambda \rangle_{\lambda_r}$ is the average flux density in the red pseudo-continuum bandpass, and λ_b , λ_r are the central wavelengths of the blue and red bandpasses, respectively.

In the rest-frame optical spectrum, widely used indices include features sensitive to both the age of stellar populations (such as the depth of the break at 4000\AA , $D_n(4000)$ and of the Balmer absorption features such as $H\gamma_A$ and $H\beta$), as well as features sensitive to the abundances of specific elements like magnesium (e.g., Mg1, Mg2, Mgb), calcium (e.g., the calcium triplet, CaT), and iron (e.g., Fe5270, Fe5335) which are calibrated to infer the metallicity of unresolved stellar populations in nearby galaxies.

A wealth of information about the metallicity of young, massive stars is also encompassed by features in the rest-frame UV region of the spectrum. In fact, they do not only reflect the composition of the photospheres of O and B stars, but also stellar winds whose strength increase with increasing metallicity due to metals dominating the opacity of the stellar material, hence allowing radiation pressure to more effectively drive material off the surface of the star. Among the most commonly analysed metallicity-sensitive, rest-frame UV stellar features are stellar-wind lines such as NV λ 1238, 1242, SiIV λ 1393, 1402, CIV λ 1548, 1550, and HeII λ 1640, or photospheric lines such as FeV λ 1360-1380, OV λ 1371, SiIII λ 1417, CIII λ 1427, FeV λ 1430, SiII λ 1533, and CIII λ 2300 (Leitherer et al., 2011). However, these features depend not only on the metallicity of stellar population, but also on factors such as stellar age and the shape of the initial mass function (IMF). Indeed, and similar to what done for rest-optical features, several spectral indices have been identified in the attempt to better isolate the metallicity dependence, by either leveraging empirical spectral libraries or sets of theoretical stellar spectra (e.g. Byler et al., 2018).

2.2.2 Full spectral fitting techniques

Over the past two decades, there has been extensive development of tools aimed at inferring multiple physical properties by reproducing the full Spectral Energy Distribution (SED) of galaxies, from ultraviolet to infrared wavelengths (see e.g. Conroy, 2013). These tools generally employ either empirical or theoretical libraries of stellar templates sensitive to different physical parameters (e.g., age, IMF, metallicity, dust, star-formation rate), which are then combined to generate a model SED which is compared to data. The model SED can either represent a ‘simple stellar population’ (SSP), describing the evolution in time of the SED of a single, coeval stellar population of a given metallicity, or combine multiple SSPs into more complex ‘composite stellar populations’ (CSPs), which contain stars with a

4 The Chemical Evolution of Galaxies

range of ages and metallicities (as well as the contribution from dust) that reflect the star-formation history (SFH) of the galaxy. Both empirical and theoretical libraries come with their own intrinsic strengths and weaknesses, and there is no single library that covers the entire range of parameter space necessary for constructing SPS models, often requiring to combine together various libraries of different quality. Theoretical libraries offer the great advantage of densely covering the parameter space, they are not limited in spectral resolution, and their model spectra are not subject to typical flux calibration issues. The disadvantage is that such libraries are only as good as the input atomic and molecular parameters, and are strongly dependent on the approximations made in the treatment of different physical processes (e.g. convection and microturbulence), as well as departures from local thermodynamic equilibrium (LTE) and from simple, plane-parallel geometry. On the other hand, empirical spectra are affected by observational constraints, being limited in wavelength coverage and spectral resolution and often largely incomplete in their probe of the physical parameter space.

These stellar population synthesis models are then fit to observational data (either broadband SEDs or spectra) to constrain multiple physical properties, including metallicity, dust attenuation, and parameters used to model the galaxy SFH. The fitting approach generally employs standard χ^2 -minimisation techniques (e.g. `PPXF`, Cappellari, 2017), or is performed within full Bayesian frameworks in which the parameter space is sampled exploiting algorithms such as Markov Chain Monte Carlo (MCMC) and the best-fit values are inferred from the marginalized posterior distributions for each parameter ¹ (e.g. `BEAGLE`, Chevallard and Charlot 2016, `BAGPIPES`, Carnall et al. 2018, `CIGALE`, Boquien et al. 2019, `PROSPECTOR`, Johnson et al. 2021).

2.3 Metallicity of the gas-phase

The metallicity of the gas-phase provides an ‘instantaneous’ snapshot of the recent SFH in galaxies, as it does not only reflect the enrichment of the gas around recently formed O and B stars, but it is also sensitive to recent gas inflows and outflows episodes. Generally, the ISM metallicity is mostly probed by its ionised phase, because the gas illuminated by young stars in HII regions produces a wealth of emission lines which are easily observable in galaxy spectra, and from which the elemental abundance of different ionic species (in particular oxygen, as discussed in Sect. 2.1) can be derived by means of different techniques, as we will briefly describe in this Section.

2.3.1 The electron-temperature method

At the base of this method lies the principle that the flux of a given emission line as observed in a galaxy spectrum is the product of the abundance of the ionic species of that given element times its volumetric emissivity. Therefore, the abundance ratio of two ions can be obtained from the ratio of the observed line intensities, once the different temperature- and density-dependence of the emissivities can be properly accounted for :

$$\frac{N(X^l)}{N(Y^m)} = \frac{I_{\lambda,X^l}}{I_{\lambda,Y^m}} \cdot \frac{J_{\lambda,Y^m}(T_e, n_e)}{J_{\lambda,X^l}(T_e, n_e)}, \quad (6)$$

where I_{λ,X^l} is the intensity of an emission line at wavelength λ for the ionic species X^l , and J_{λ,X^l} is the emissivity. When deriving the relative abundances of specific metal ionic species (for instance, doubly-ionized oxygen, O^{++}) to hydrogen, the above formula becomes

$$\frac{O^{++}}{H^+} = \frac{I([\text{O III}]\lambda 5007)}{I(H\beta)} \cdot \frac{J_{H\beta}(T_e, n_e)}{J_{[\text{O III}]}(T_e, n_e)}, \quad (7)$$

where it is common practice to measure line strengths relative to $H\beta$ because this line is readily observed and generally not blended with other lines even at lower spectral resolutions. Most emission lines from metal ionic species at optical wavelengths are forbidden lines arising from collisional excitation (CEL), with critical densities² generally much higher than the density of medium they originate from. In such circumstances, the volumetric emissivity of the transition is given by

$$J_\lambda = h\nu_{ul} \frac{n_u A_{ul}}{4\pi} \sim n_e n_x e^{-E_{ul}/kT_e}, \quad (8)$$

where n_e is the density of electrons (i.e. the ‘colliding particles’), n_x the density of the ion X , u and l the upper and lower levels of the transition, and A the Einstein coefficient for spontaneous emission, hence showing that J_λ has an exponential dependence on temperature. On the contrary, the temperature-dependence of the volumetric emissivity of a permitted, recombination line such as $H\beta$ is only (approximately) linear. Therefore, when comparing the intensity of a CEL to that of a recombination line to infer ionic abundances, one needs to account for the fact that the ratio of the volumetric emissivities is a strong function of temperature (and, though more mildly, of density), hence the application of this method (often known as the ‘ T_e -method’) requires accurate knowledge of both electron temperature T_e and density n_e of the emitting nebula. The total elemental abundance is then obtained by co-adding the individual ionic abundances, and correcting for those not directly observed by means of specific ‘ionization correction factors’ (ICF).

Temperature and density diagnostics

The structure of the energy levels of some ionic species is such that the ratio between different optical emission lines can be employed as temperature or density diagnostics. For instance, the energy-levels configuration of the O^{++} ion is represented in the left panel of Fig. 1. All the levels above the ground state are populated by the excitation due to the collisions between ions and free electrons. The

¹however, care should always be taken in considering the (sometimes significant) influence that the specific choice of the priors can have on the inferred best-fit values

²defined as the density at which the rate of collisional de-excitations equals the rate of spontaneous radiative transitions

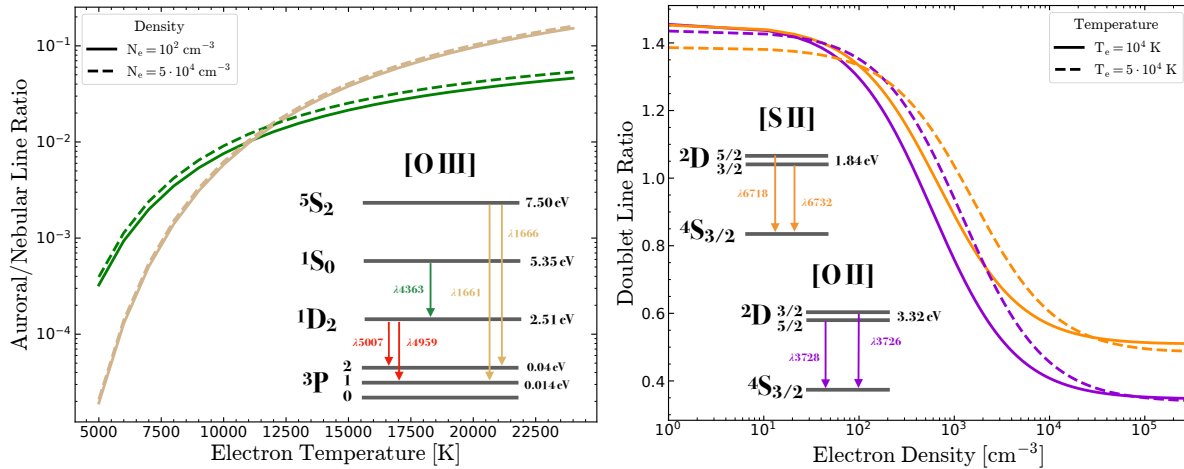


Fig. 1 Examples of diagnostics of the ISM. The left-hand panel reports the behavior of different [OIII] auroral-to-nebular line ratios as a function of temperature, namely [OIII] λ 4363/[OIII] λ 5007 and [OIII] λ 1661, 1666/[OIII] λ 5007. Each curve is plotted for two very different electron density regimes, demonstrating the small residual dependence on N_e . The Grotrian diagram for [OIII], highlighting the involved transitions, is plotted in the bottom-right part of the panel. The right-hand panel shows instead two classical density diagnostics, namely the [OII] λ 3727/[OII] λ 3729 and [SII] λ 6718/[OII] λ 6732 doublet line ratios. The curves are plotted for two different T_e values, and the Grotrian diagrams of the involved transitions are also shown.

relative populations of the ^1S and ^1D states depend critically on T_e , hence the ratio between emission lines arising from these levels will be highly temperature-sensitive. For instance, in nebular and galaxy evolution studies the [OIII] λ 4363/[OIII] λ 5007 ratio is one of the most commonly adopted diagnostics of electron temperature. We note that in this context lines originating from the highest energy levels (e.g. [OIII] λ 4363, or the rest-frame UV [OIII] λ 1661, 1666) are often referred to as ‘auroral lines’; such emission lines are generally much fainter than ‘nebular’ transitions (e.g. [OIII] λ 5007), down to a factor of \approx a few hundredths at high metallicity³, hence often representing the biggest observational limitation to the application of the T_e -method. Other common T_e diagnostics involving different ionic species (and probing different ionization states of the gas) include the [NII] λ 5755/[NII] λ 6584, the [OII] λ 7320, 7330/[OII] λ 3727, 3729, and the [SIII] λ 6312/[SIII] λ 9530 line ratios. From detailed calculations of (approximated) 5-level atom structures, numerical formulae to measure the electron temperature from the observed line ratios are derived; however, we note that these expressions depends on the assumed collision strengths of the transitions, which are generally tabulated for the typical range of nebular conditions but can vary between different versions of atomic datasets.

The electron density n_e can be measured instead exploiting ratios of emission lines originating from excited states of similar energy (hence emitted in wavelength-close doublets), but different critical densities for collisional de-excitation. These ratios are sensitive to n_e (while almost insensitive to temperature) in the regime comprised between the critical densities of the two transitions, while saturate in both lower and higher density regimes. Typical density diagnostics for HII regions in rest-frame optical are the [OII] λ 3727, 3729 and [SII] λ 6717, 6731 doublets (right-hand panel of Fig. 1), while diagnostics in the rest-frame UV, sensitive to higher density regimes, include e.g. the [CIII] λ 1907, 1909 and [NIV] λ 1483, 1485 doublets.

Caveats on the T_e -method

A number of assumptions underlines the application of the T_e -method. Since forbidden, collisionally-excited lines are optically thin, any flux measurement represents emissivity-weighted averages along the line of sight through the nebula. Although in the case of reasonably homogeneous conditions the measured electron temperature is representative of the average temperature of the nebula, inhomogeneities in the form of temperature and density fluctuations can instead severely bias the interpretation of the inferred temperature. It is indeed well known that HII regions are far from being homogeneous: on the contrary, pockets, filaments, and shells with different n_e and T_e structures are clearly observed (Méndez-Delgado et al., 2023a; Kreckel et al., 2024). In regions where T_e is enhanced, the emissivity of the temperature-sensitive auroral lines is disproportionally enhanced over that of the stronger nebular lines: this translates into an overestimation of the average T_e , leading to an underestimation of the metallicity when integrating the line ratios over the whole nebula. Such effect is even more prominent when considering global, integrated galaxy spectra which are the result of averaging over multiple HII regions of different properties, and which make the interpretation of metallicity as measured in galaxy spectra not straightforward (Pilyugin et al., 2010). The advent of integral-field-spectroscopy (providing spatially-resolved spectral information for both nearby and distant galaxies) marked great advancements in this regard.

³gas temperature and metallicity are tightly correlated, as emission lines from metal ions are the primary cooling channels of the ISM

Abundances from recombination lines and the ‘Abundance Discrepancy Factor’

In principle, the most ‘direct’ probe of elemental abundances would follow by comparing recombination lines (RL) of metal ions with those of hydrogen. In fact, the similar dependence of the involved emissivities on both n_e and T_e would make the ratio between RLs of different ions only proportional to the relative abundances, while almost independent on the gas density and temperature conditions, hence more robust against the typical biases of the T_e -method associated with temperature fluctuations (e.g. Peimbert and Peimbert, 2014). However, this also means that RLs of metal species are extremely faint (of the order of 10^{-3} - 10^{-4} times the intensity of Balmer lines, even for the most abundant elements like carbon and oxygen): therefore, the detection of metal RLs and their applicability in abundance measurements is practically limited only to bright and nearby HII regions, planetary nebulae, and supernova remnants in the Milky Way (MW) and the Local Group (e.g. García-Rojas and Esteban, 2007), and requires spectra of high-resolution and high signal-to-noise ratio.

Notably, chemical abundances measured via RLs have been widely observed to deviate from those based on the T_e -method, with typical discrepancies up to a factor of ~ 0.3 dex. The origin of such disagreement, also known as ‘Abundance Discrepancy Factor’ (ADF, see e.g. Peimbert et al., 2017; Toribio San Cipriano et al., 2017), is still currently debated. On the one hand, temperature fluctuations are invoked as the main culprits, affecting, as seen, mostly T_e measurements, and inducing an underestimate of the real metallicity (Peimbert, 1967; Méndez-Delgado et al., 2023b). On the other hand, there also are indications, based on the comparison with fine-structure infrared lines such as [OIII] λ 52, 88 μ m, that temperature fluctuations might not be the main responsible for the ADF (Tsamis et al., 2003; Chen et al., 2023). In fact, the presence of small-scale, chemical inhomogeneities due to a clumpy, not well mixed gas distribution might possibly explain the different results arising from RLs (dominated by the metal-rich clumps) and the CELs (dominated by more diffuse medium) measurements (Stasińska et al., 2007). Furthermore, spectroscopy performed on individual, supergiant stars in nearby spiral galaxies suggest that T_e -based abundances are in better agreement with stellar metallicities (once taking into account the depletion onto dust) than those measured from recombination lines, especially in metal-poor environments (Bresolin et al., 2016).

2.3.2 Statistical (strong-lines) methods

Auroral lines involved in the classical T_e -method are generally faint and their emissivity is strongly temperature-dependent, making them extremely challenging to detect, especially in high-metallicity systems. This practically limits the applicability of ‘direct’ metallicity measurements to a relatively small sample of galaxies, which either low-metallicity and/or high signal-to-noise spectra brings such faint emission line fluxes within the reach of current facilities. Although the number of spectra with auroral lines detections have increased significantly (also at high redshift) over the past years thanks to the improvement in the astronomical instrumentation, they still represent a tiny fraction of the global galaxy population. Therefore, alternative methods need to be developed to study the metallicity properties of large galaxy samples like those probed by extensive spectroscopic surveys.

These techniques generally employ the (either direct or secondary) dependence of some line ratios between bright emission lines and metallicity (or, more specifically, oxygen abundance), and are referred to as the ‘strong-line methods’. Such a dependence can derive from the correlation between metallicity and electron temperature of the gas, or be driven by more indirect correlations between the metallicity and ionization parameter or through the relative abundances of different chemical species (like the nitrogen-to-oxygen ratio, e.g. Pérez-Montero and Contini 2009). Such ‘strong-line’ diagnostics are generally calibrated against ‘direct’ oxygen abundance measurements in sample of individual galaxies (or exploiting spectral stacking, e.g. Curti et al. 2017) for which the T_e -method can be adopted. When applied to different galaxy spectra they must be therefore interpreted in a ‘statistical’ sense, and the inferred metallicity should be considered reliable only if the physical properties of the target match those of the calibration sample.

The majority of the most popular strong-line diagnostics involves rest-frame optical line ratios, leveraging the presence of many bright transitions in this wavelength range and its accessibility. Among multiple diagnostics proposed and calibrated in the past, some relies uniquely on a combination of oxygen and hydrogen lines (such as $R_{23} = ([\text{OIII}]\lambda\lambda 4959, 5007 + [\text{OII}]\lambda\lambda 3727, 29)/\text{H}\beta$ and $R_3 = [\text{OIII}]\lambda 5007/\text{H}\beta$) and are thus primarily sensitive to the oxygen abundance, though showing a double-branched behavior due to the different relative importance of optical CELs in regulating the ISM cooling in different metallicity regimes⁴ (Pagel et al., 1979; McGaugh, 1991). Several authors hence proposed to use combinations of multiple diagnostics to break the degeneracy in the metallicity solution, leveraging the monotonic (though often ‘secondary’) dependence on oxygen abundance of line ratios such as $O_{32} = ([\text{OIII}]\lambda 5007/[\text{OII}]\lambda\lambda 3727, 29)$ (sensitive primarily to the ionization parameter, Kobulnicky and Kewley 2004), $N_2 = [\text{NII}]\lambda 6584/\text{H}\alpha$ and $O_3N_2 = R_3 - N_2$ (which introduce a direct dependence on the nitrogen abundance, hence their interpretation as oxygen abundance tracers is sensitive to the distribution in N/O of the calibration sample, Pettini and Pagel 2004). Additional diagnostics involving emission lines of different elements leverage the proximity in wavelength to reduce the impact of uncertainties on the reddening correction, and include e.g. $\text{Ne}_3\text{O}_2 = [\text{NeIII}]\lambda 3869/[\text{OII}]\lambda\lambda 3727, 29$ (Nagao et al., 2006), $N_2S_2\text{H}\alpha = [\text{NII}]\lambda 6584/[\text{SII}]\lambda\lambda 6717, 31 + 0.22 [\text{NII}]\lambda 6584/\text{H}\alpha$ (Dopita et al., 2016), $S_2 = [\text{SII}]\lambda\lambda 6717, 31/\text{H}\alpha$ and $R_3S_2 = R_3 + S_2$ (Curti et al., 2020b). Each of these diagnostics carries both advantages and disadvantages, related to the relative strength of the lines involved, their wavelength separation (and hence reddening sensitivity), and dependence on other chemical elements or physical parameters rather than oxygen abundance: therefore, combining multiple diagnostics represents often a valuable approach to marginalize over these different effects. For a more thorough discussion on strengths and weaknesses of the hereby discussed (and more) strong-line diagnostics, we refer to the review by Maiolino and Mannucci (2019).

⁴At high metallicities, the most efficient cooling channel is represented by the infrared [OIII] 88 μ m emission, which lowers the temperature below the excitation threshold of optical CELs. Thus, since T_e decreases with increasing O/H, [OIII] λ 5007/H β decreases with oxygen abundance in this regime. At lower metallicities instead, T_e is higher, powering the collisional excitation of the [OIII] λ 5007 line, which becomes the dominant coolant: this represents an intermediate regime where diagnostics such as R_3 and R_{23} are almost independent of O/H. Finally, at very low metallicity cooling is dominated by recombination, and collisional excitation of [OIII] λ 5007 scales proportionally with O/H.

2.3.3 Photoionisation models

Beside strong-line diagnostics calibrated ‘empirically’ over samples of observed galaxy spectra, extensive development in the area of photoionisation modeling over the past years culminated in a broad set of theoretical frameworks aimed at determining the physical properties of galaxies (including metallicity) via simultaneous fitting of multiple emission line features. The classical approach is to use photoionization codes such as CLOUDY (Ferland et al., 2017) or MAPPINGS (Dopita et al., 1996), possibly adopting different types of input ionizing radiation, to generate multiple grids of emission line ratios whose dependence upon gas properties such as ionization parameter⁵ and gas-phase metallicity can be fully modeled and explored (e.g. Kewley and Dopita, 2002; Dopita et al., 2013; Gutkin et al., 2016).

More recently, this approach has been frequently incorporated into full SED fitting codes (already discussed in Section 2.2.2) to simultaneously constrain stellar and nebular properties within robust Bayesian frameworks. The effect of dust is also generally included, both in terms of attenuation (sometimes also distinguishing the contribution from the dense clouds where stars are born from the that of the diffuse ISM, e.g. Chevallard and Charlot 2016) and of differential depletion of chemical elements. The flexibility of these codes allows to probe a large number of galaxy properties over wide dynamic ranges, beyond those typically accessible by the majority of empirical calibration samples (especially at high redshift), and to have a good handle on the parameters’ uncertainties, degeneracies, and correlations, although being intrinsically tied to the assumptions of the underlying model grids.

Despite the very high potential in fact, photoionisation models suffer from a number of limitations associated for instance with oversimplified geometrical configurations (with HII regions often modeled as plane-parallel slabs of gas), relative chemical abundances assumed to scale proportionally to the solar pattern or by means of fixed relationships with no-scatter, uncertainties on the input stellar libraries (though extensive work has been done recently to include for instance the effect of binaries and stellar rotation, e.g. Stanway and Eldridge 2018), and constant dust-to-metal ratios with both metallicity and redshift. This often translates into the inability for a given model to match simultaneously all the observed line ratios for an individual galaxy with the same, fixed set of parameters, although the statistical distribution of galaxy samples within specific diagnostic diagrams is generally well reproduced.

Furthermore, the metallicity inferred from photoionization models is generally overestimated compared to that derived by means of more ‘direct’ methods such as the T_e -method, with discrepancies that can reach up to ~ 0.6 dex, especially in the high metallicity regime (Kewley and Ellison, 2008). Among the possible sources of discrepancies, there are a different treatment of dust depletion (which models generally account for, whereas ‘direct’ measurements only probe metals in the gas-phase) and temperature fluctuations in real nebulae (see Section 2.3.1), possibly producing an underestimate of the ‘true’ abundances with the T_e -method on the one hand, as well as some of the simplistic models’ assumptions discussed above (for instance related to the scaling of nitrogen-to-oxygen abundance, Nicholls et al. 2017) on the other. Regardless of which can be deemed as the ‘true’ absolute values (although T_e -measurements are generally considered more physically motivated, as inferred from real observations of nebular spectra and descending from basic concepts of atomic physics), it is warranted to stress the importance of sticking to the same, self-consistent abundance scale when performing comparative studies in the literature, as hybrid combinations of model- and T_e -based calibrations can introduce subtle systematics effects as a function of metallicity which might hamper the correct interpretation of the observations.

2.4 Absorption line techniques

If a gas cloud is observed against a bright background source of radiation (e.g. a distant quasar), the absorption produced by a given transitions provides a direct measurement of the column density of the associated ionic species. Combined with a measurement of the hydrogen column density through one of the Lyman absorption lines, and modulo properly accounting for the different ionization states of the gas, it is possible to obtain very accurate measurements of the metallicity as well as of relative chemical abundances of different elements. These techniques offer several advantages, including being sensitivity to extremely low column densities (down to $N \approx 10^{12} \text{ cm}^{-2}$), and the possibility to probe a wide range of densities (unlike emission-lines which intensity scales as $\approx N^2$), redshifts, and target luminosities. On the other hand, absorption studies provides only projected measures of the gas surface density, and are usually limited to one sightline per galaxy given the rarity of background quasars.

Absorption line techniques can probe systems across a large range of column density regimes. Up to column densities of $\log(N/\text{cm}^2) \approx 16$, absorption profiles can be studied by directly measuring the equivalent width of the line, whereas at higher densities saturation effects starts to become relevant, often providing only lower-limits on the inferred column density of the ionic species and requiring to fit high-order Lyman series lines to derive the hydrogen column density. Systems with $\log(N_{\text{HI}}/\text{cm}^{-2}) > 16.2$ are referred to as ‘Lyman limit systems’ (LLS), as they cause a clear drop-off in the measured flux at the Lyman limit of 912 \AA , and typically probe the dense part of the CGM of galaxies (see Section 4.4). Above $\log(N_{\text{HI}}/\text{cm}^{-2}) \gtrsim 20.3$, the highest Lyman series lines are saturated, and column densities must come from fitting of the $\text{Ly}\alpha$ profile, which on the contrary starts showing clear signatures of damped wings: these are so-called ‘damped Lyman- α ’ (DLA) systems, and represent the class of systems most widely exploited to trace metal enrichment through absorption features at cosmological distances (e.g. Pettini, 2004; Poudel et al., 2018). It is worth noting that, even in those cases in which the optical counterpart of the absorber is identified, it is not straightforward to associate the DLA system with a specific region of a galaxy, e.g. whether it is tracing the ISM in the outer disks or dense gas clumps within the galaxy’s circumgalactic medium (CGM). Nonetheless, the process of associating absorbing systems with emitting galaxies have made huge progress in the last decade, especially thanks to last generation IFU instruments such as VLT/MUSE (e.g. Lofthouse et al., 2020) and KECK/KCWI (e.g. Martin et al., 2019).

Since these observations generally probe atomic hydrogen and a fraction of the metal ionic states along any given line-of-sight, some-

⁵The ionization parameter is defined as the dimensionless ratio of the number of ionizing photon emitted per unit time Q_{ion} to the gas density, normalized by the speed of light, i.e. $U = Q_{\text{ion}}/(4\pi r^2 n_e c)$, where r is generally calculated as the distance to internal surface of the illuminated cloud.

8 The Chemical Evolution of Galaxies

times significant ionization corrections are required to move from a measured ratio of ionic to HI column density $N(X^i)/N(H^0)$ to an abundance ratio $[X/H]$. Ionization correction factors are generally estimated from photoionisation codes like CLOUDY (Ferland et al., 2017), assuming simple geometrical configurations with an ionizing radiation field incident on a plane-parallel slab of constant density gas. At the large column densities probed by DLA systems however, the optical depth is large enough for the interior of the cloud to be self-shielded from the external radiation field, hence the gas is predominantly in the neutral phase and chemical abundance measurements require little ionization corrections.

Finally, a robust measurement of the metal content with absorption line techniques also requires to account for depletion of metals onto dust grains. This process is differential, as some elements are more likely to be incorporated into dust grains based on their chemical properties: for instance, over 50% of metals in the Milky Way's ISM are in the solid phase, but elements like Fe are extremely depleted with up to 90 – 99% of the total abundance incorporated into dust. Neutral absorbers show differential depletion patterns similar to, but less severe than, those in the Milky Way. Evidence of metal depletion extends to high-redshift systems, and indicators of dust presence, such as the 2175Å absorption bump (Witstok et al., 2023) and strong infrared absorption features (Aller et al., 2014), further confirm the presence of solid-phase material in these environments. While early studies focused on lightly depleted elements, such as zinc (Zn) and silicon (Si), to estimate total metal abundances (e.g. Pettini et al., 1997), more recent works have used empirically-calibrated depletion patterns to correct gas-phase measurements, deriving more accurate total metal abundances (Jenkins, 2009; De Cia et al., 2018).

3 Chemical Evolution Models

The chemical enrichment in galaxies is regulated by the complex interplay of multiple physical processes occurring on different spatial and temporal scales. These include gas accretion from the cosmic web, stellar evolution and nucleosynthesis, stellar winds and SNe explosions, gas outflows (possibly removing gas from the galaxy), gas recycling from the surrounding CGM, dust creation and destruction, AGN activity, dynamical interactions and mergers. Over the past decades, detailed analytical and numerical frameworks aimed at describing the impact (and relative role) of all these processes in driving galaxy evolution and, more specific to this context, at predicting the observational signatures in their chemical enrichment patterns, have been extensively developed. Despite a variety of different approaches, assumptions, and levels of complexity, most of these models lie on the foundation of simple equations describing galactic chemical evolution (GCE), and involve a number of common relevant parameters, as described in the following.

3.1 Analytical models

Analytical models of galactic chemical evolution generally attempt to describe the interplay between four main processes, described by means of as many parameters: gas accretion, the efficiency of gas conversion into stars (star formation efficiency), the amount of metals produced by stars and returned to the ISM (stellar yield), and the amount of gas lost from the system due to stellar winds and outflows. Of particular relevance is the definition of stellar yields, which are derived from models of stellar evolution. The yield is defined as the fraction in mass of a given element produced per unit mass of stars formed and returned to the ISM; yields therefore depend on the mass of the star, its chemical composition, and other properties such as stellar rotation. For instance, a supernova originating from a $35 M_{\odot}$ star produces $\approx 5 M_{\odot}$ of oxygen and $\approx 1 M_{\odot}$ of carbon (Chieffi and Limongi, 2004). When modelling GCE, yields are computed for full simple stellar populations (i.e. for stars formed at the same time) by integrating the yields of individual stars over the initial mass function (IMF). These yields depend on the ISM enrichment at the time of the formation of the stellar population and, possibly, also on time, to reflect any cosmic evolution in the IMF. Throughout the simple treatment of GCE within this Chapter, we will work under the assumption of a constant IMF.

In classical models, the equations describing a galactic system can be simplified under the assumption that stars can be divided into two classes: those that live forever (with M_{\star} below some threshold, $M_{\star} < M_0$) and those that die out as soon as they are born ($M_{\star} > M_0$): this is known as ‘instantaneous recycling approximation’ (IRA). Such approximation is justified by the fact that most of the metals are produced by Type II SNe of massive stars progenitors ($\geq 8 M_{\odot}$) with short lifetimes of \approx a few Myrs. However, these models fall short in capturing the full chemical evolution of elements like iron (Fe), whose enrichment occur on much longer timescales (\approx Gyrs) due to significant contribution from type Ia SNe.

Under the IRA conditions (and assuming the metallicity Z is always $\ll 1$, hence the mass in metals can be ignored compared to the total gas mass), the basic equations describing galactic chemical evolution can be expressed as :

$$\frac{dM_s}{dt} = (1 - R)\psi ; \quad \frac{dM_g}{dt} = -(1 - R)\psi + \phi - \omega ; \quad \frac{d(ZM_g)}{dt} = -Z(1 - R)\psi + y(1 - R)\psi + Z_{\phi}\phi - Z\omega ; \quad (9)$$

where M_s is the mass in stars, M_g is the mass in gas, ψ is star-formation rate (i.e. the amount of stellar mass formed per unit time), ϕ is the gas infall rate, ω is the outflow rate (with both ϕ and ω which are functions of time), R is the ‘return fraction’ (i.e. the fraction in mass returned to the ISM per stars formed, which depends on the IMF), y is the yield, Z is the metallicity of the ISM, Z_{ϕ} is the metallicity of the infalling gas, while the metallicity of the outflowing gas is the same as that of the ISM. Generally, the last equation can be written explicitly in terms of the metallicity Z (instead of the total mass of metals in the gas-phase, ZM_g),

$$M_g \frac{dZ}{dt} = y(1 - R)\psi + (Z_{\phi} - Z)\phi . \quad (10)$$

The closed box model

The simplest realisations of GCE models assume that all the gas is already present initially and is pristine (no gas inflows, $M_g(t=0) = M_0$, $Z(t=0) = 0$), that metals are produced, returned, and mixed into the ISM, and that this enriched gas forms the next generations of stars without any loss of gas (no outflows): these are generally referred to as ‘closed box models’, and explore the evolution of only three quantities, i.e. the gas mass M_g , the stellar mass M_s , and the metallicity Z . Since the total mass in the systems remains constant with time, i.e. $M = M_s + M_g = M_0$, integrating the equations 9 and 10 leads to

$$Z = y \ln \mu_g^{-1} \quad (11)$$

where $\mu_g \equiv M_g/(M_g + M_s) = M_g/M_0$ is the ‘gas fraction’ of the system. Therefore, in this model the metallicity increases monotonically as the gas mass decreases due to star formation. To fully solve the closed box model we need to specify how efficiently gas is converted into stars, which we parametrize as the ‘star-formation efficiency’ $\tau = M_g/\dot{M}_s$, here assumed constant over time⁶. Because at any given time the variation in the gas mass corresponds to an opposite variation in the stellar mass (i.e. $\dot{M}_g = -\dot{M}_s$), we obtain the following expressions describing the temporal evolution of gas mass and star-formation rate

$$M_g(t) = M_g(0) e^{-t/\tau}; \quad \dot{M}_s(t) = \frac{M_g(0)}{\tau} e^{-t/\tau}. \quad (12)$$

The metallicity evolution is then given by

$$Z(t) = -y \cdot \ln \left[\frac{M_g(t)}{M_g(0)} \right] = y \frac{t}{\tau}. \quad (13)$$

From equation 13 we see that the metallicity reaches its peak $Z = y$ at $t = \tau$. Applying this scenario to the Milky Way, assuming the present-day measured gas fraction of the Solar neighborhood $\mu_g = 0.1$ and a solar metallicity $Z_\odot = 0.014$ (Asplund et al., 2009), we derive a yield $y \sim 0.006$ and a timescale for peak metallicity of $t = \tau Z_\odot / y \approx 2.33\tau$.

Comparing the closed box model predictions with observations however immediately highlights several critical aspects of its over-simplified approach. For instance, the stellar yield value inferred as above is significantly lower than the typical yields computed from stellar evolution at solar metallicity ($y \sim 0.035$). Furthermore, the metallicity distribution predicted by the closed box model includes a much larger number of low-metallicity stars than observed in the solar neighborhood: in fact, the model predicts a mass fraction of stars of metallicity below 25% solar of $M_s[Z < 0.25Z_\odot] \sim 0.45$, whereas the observed value is ~ 0.02 . The origin of such disagreement (also known as the ‘G-dwarf problem’) resides in the fact that early star formation and enrichment produces an amount of metals which is diluted by the large gas reservoir required to sustain star-formation throughout the life of the system (indeed, we recall that in closed box models all the gas is immediately available to form stars). Therefore, the metallicity initially grows slowly, and many stars therefore form from low-metallicity gas for a long time. As the gas reservoir starts to get exhausted with time, star formation produces the same yield of heavy elements, which however enrich an ever smaller amount of gas such that significantly fewer stars form in relatively high metallicity ranges. A possible solution to this problem is to model galaxies as ‘open systems’, including the contribution from gas inflows and outflows in our prescriptions.

The impact of gas flows

It is relatively straightforward to understand that galaxies are far from being ‘closed boxes’. On the one hand in fact, they accrete gas from their cosmic environments, while on the other gas can be removed by winds driven by either massive stars, supernova explosions, and active galactic nuclei.

Typically, the amount of gas lost due to outflows per unit time (the ω term in equation 9) is parameterized in terms of the ‘mass loading factor’ η , expressed as a fraction of the star-formation rate $\psi \equiv \dot{M}_s$

$$\omega \equiv \dot{M}_{\text{outflow}} = \eta \dot{M}_s, \quad (14)$$

which implicitly assumes that outflows are primarily driven by the winds or supernova explosions of massive stars. Incorporating outflows in the equations of the closed box model, we obtain

$$\dot{M}_g = -\dot{M}_s - \dot{M}_{\text{outflow}} = -(1 + \eta) \dot{M}_s \quad (15)$$

for the evolution of the gas mass, whereas the amount of mass in metals M_Z evolves as

$$\dot{M}_Z = (y - Z) \dot{M}_s - Z \dot{M}_{\text{outflow}} = (y - Z - \eta Z) \dot{M}_s. \quad (16)$$

Combining equations 15 and 16, and expressing everything in terms of metallicity Z , we obtain

$$\frac{dZ}{dt} = -\frac{y}{1 + \eta} \frac{\dot{M}_g}{M_g}, \quad (17)$$

⁶Note that a larger value of τ corresponds to a longer time required to consume the available gas, hence to a lower efficiency of star formation

hence

$$Z(t) = -\frac{y}{1+\eta} \ln \left[\frac{M_g(t)}{M_0} \right] \equiv y_{\text{eff}} \ln \mu_g^{-1}, \quad (18)$$

where we have defined the ‘effective yield’ $y_{\text{eff}} = y/(1+\eta)$ in order to recover the same functional form for the evolution of the metallicity Z as in the closed box model (cfr. equation 11): here, the effective yield is lower by a factor $1+\eta$ than the metal yield of the stellar population to account for the fraction of enriched gas expelled from the galaxy. This class of models takes the name of ‘leaky box models’ and allow, for example, to reconcile the predicted and measured values of the stellar yields (by taking $\eta \approx 5$), as well as to bring the expected number of low-metallicity stars in better agreement with observations. The inclusion of gas outflows in more detailed realisations of GCE models allows to successfully reproduce some of the most relevant scaling relations observed in galaxy populations, such as the mass-metallicity relation (Tremonti et al., 2004, see Section 4.1.1), which is indeed predicted to be driven by a decreasing efficiency of outflows in higher mass galaxies (characterised by increasingly higher escape velocities due to their deeper gravitational potentials) leading to increasing metallicity as a function of stellar mass.

Alternatively (or in addition), we can incorporate a term which reflects the accretion of gas from the cosmic web providing the supply for star-formation. Indeed, many cosmological frameworks predict that gas accreted in the form of cold streams is the main driver of galaxy assembly (Dekel et al., 2009). Including gas accretion into the equations of closed box models give rise to the so-called ‘accreting box models’. In their simplest form, we can assume that the accretion of gas perfectly balance the gas consumed by star-formation rate ($\phi = (1-R)\psi$), such that the total gas mass remains constant with time ($\dot{M}_g = 0$). Substituting this into equations 9, and under the additional assumption of pure pristine gas accretion (i.e. the metallicity of the infalling gas is equal to zero), we obtain

$$\dot{Z} = (y - Z) \frac{\dot{M}_s}{M_g} \quad (\text{since } \dot{M}_g = 0) \quad (19)$$

and, by means of a change of variable from time to the total mass of the system $M = M_g + M_s$, and considering that $\dot{M} = \dot{M}_s$, we have

$$\frac{dZ}{dM} = \frac{\dot{Z}}{\dot{M}_s} = \frac{(y - Z)}{M_g}. \quad (20)$$

In the scenario of zero initial metallicity ($Z(0) = 0$) and $M(0) = M_g$, a possible solution is in the form

$$Z = y \left[1 - \exp \left(1 - \frac{M}{M_g} \right) \right]. \quad (21)$$

In such a model, the total mass quickly becomes larger than the gas mass right after the beginning of star-formation (which is fueled by external accretion), and for $M \gg M_g$ the metallicity of the system reaches $Z \approx y$, representing the equilibrium value between enrichment and pristine accretion which is directly set by the stellar yield. The accretion box models provides better agreement between both the inferred ($y \approx 0.014^7$) and observed ($y \approx 0.035$) yields as expected from stellar evolution, as well as for the fraction of low-metallicity stars in the solar neighborhood.

We have seen therefore how including the contribution of gas flows (in the form of pristine cosmological gas accretion and/or gas removal from outflows) into a closed box system helps to reconcile models predictions with observations. In general, advanced analytical chemical evolution models account for both processes in their frameworks. A widely adopted class of models assume that gas inflow is compensated by star formation and outflows, yielding a quasi-steady state in which the gas content only slowly varies with time: these are hence known as ‘equilibrium’ or ‘gas-regulator’ models (e.g. Peebles and Shankar, 2011; Lilly et al., 2013). These models have proven successful in reproducing multiple average properties of galaxy populations, in particular the metallicity scaling relations, which in turn provide some of the most relevant observational constraints to the models’ parameters and, in turn, to the mechanisms regulating star-formation and mass assembly in galaxies that such parameters describe.

3.2 Numerical models and simulations

These models simulate the hierarchical growth of cosmic structures via cosmological accretion and merging, starting by N-body simulations tracking the effects of gravity on both dark and baryonic matter. Key elements in these models are the spatial (and mass) resolution and the total size of the simulation, the latter related to the total number of particles and the volume of the Universe being probed. Due to highly demanding computational resources of these simulations, it is almost never possible to simultaneously study larger volumes at high-resolution. Therefore, although in many cases the share the same underlying physical principles, different simulations are run probing a range of different resolutions and sizes depending on their primary scientific objectives. Among notable examples of large scale, cosmological simulations of galaxy formation and evolution implementing also chemical enrichment processes, we mention ILLUSTRIS (Vogelsberger et al., 2014), ILLUSTRIS-TNG (Nelson et al., 2019), EAGLE (Schaye et al., 2015), HORIZON-AGN (Dubois et al., 2014), FIRE (Hopkins et al., 2014), and MUFASA (Davé et al., 2017), whereas hybrid, semi-analytical approach is followed by the L-GALAXIES simulations (Henriques et al., 2020). Extremely detailed, high-resolution simulations of individual galaxies are instead provided e.g. by SERRA (Pallottini et al., 2017) and RAMSES (Katz, 2022). For a more comprehensive overview we refer to Somerville and Davé (2015).

⁷assuming the Milky Way’s present-day gas fraction and solar metallicity

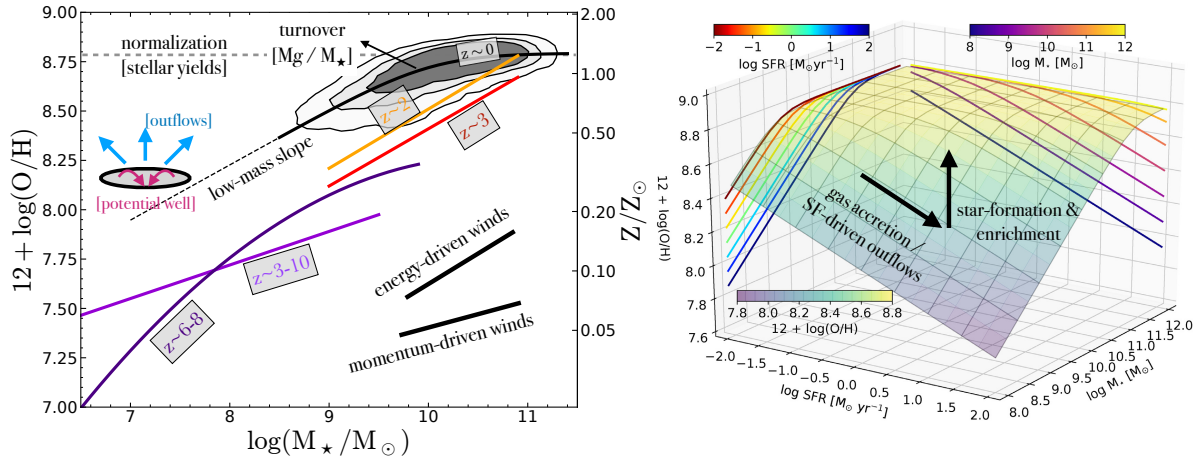


Fig. 2 Gas-phase metallicity scaling relations. Left Panel: Mass-Metallicity Relation (MZR) as observed in the local Universe (grey contours, $z \sim 0.08$, Curti et al. 2020b), and for different samples at high-redshift ($z \sim 2 - 3$ from Sanders et al. 2021; $z \sim 3 - 10$ from Curti et al. 2024a; $z \sim 6 - 8$ from Chemerynska et al. 2024). Some of the physical processes responsible for shaping the relationship are schematized, and the slopes predicted by assuming either ‘energy-driven’ or ‘momentum-driven’ winds are also overlaid (with arbitrary normalization). Right Panel: Graphical representation of a possible parametrisation of the FMR surface in the 3D space given by M_* , SFR, and O/H. The colour-coding of the surface reflects the predicted metallicity, and the contours of the projections of the FMR onto the M_* -O/H and SFR-O/H planes are also drawn. Adapted from Curti et al. 2020b.

4 The observational landscape

Few research areas in astronomy have experienced the same progress over the past two decades as the study of the chemical evolution of galaxies. Major advancements in observational techniques and the advent of both ground- and space-based cutting-edge facilities with high sensitivity, high multiplexing, and wide wavelength coverage have in fact enabled to probe the chemical evolution in large galaxy samples, map their metal content, and directly probe the enrichment process of galaxies and of the intergalactic/circumgalactic medium up to the earliest cosmic epochs, setting tight constraints on models of galaxy formation. In this Section we provide a brief overview of the current observational landscape regarding the study of the metallicity scaling relations, the relative abundances of chemical elements, and their spatial distribution in and out of galaxies, trying to connect these results over a wide range in cosmic history.

4.1 Metallicity scaling relations

The incessant interplay between gas flows, star-formation, and metal enrichment that regulates the baryon cycle leaves clear signatures on both stellar and ISM metallicity. Observationally, this is reflected into the existence of scaling relations between metallicity and other global galaxy properties, whose investigation can help shedding light onto the relative role that these processes have in driving galaxy evolution.

4.1.1 The Mass-Metallicity Relation

The most evident and thoroughly studied scaling relation relates the total stellar mass with the metal content in galaxies, and is known as the ‘Mass-Metallicity Relation’ (MZR), and it is observed for both stellar and gas-phase metallicity. Observationally, the MZR in the gas-phase is a rather tight correlation (~ 0.1 dex scatter) in which the more massive systems appear more metal enriched. Initially suggested in the form of a correlation between metallicity and luminosity in irregular and blue compact galaxies (Lequeux et al., 1979), it was then fully characterised with the advent of large spectroscopic surveys like the Sloan Digital Sky Survey (SDSS York et al., 2000), which allowed to study the MZR over three orders of magnitude in stellar mass (Tremonti et al., 2004; Andrews and Martini, 2013; Curti et al., 2020b) and even down to the regime of dwarf galaxies (Lee et al., 2006; Yates et al., 2020), despite such low-mass regime being more prone to sample selection biases (Scholte et al., 2024).

The MZR presents a relatively steeper slope at low and intermediate masses, while evidence for a turnover and flattening in the high-mass regime is observed. The main features of the MZR, i.e. the slope, turnover mass, and normalisation, can be linked to different physical processes, and their characterisation provides some of the most powerful constraints on galactic chemical evolution models (left-hand panel of Fig. 2). The MZR slope reflects feedback mechanisms in galaxies as shaped by star-formation-driven outflows and, in particular, how the mass-outflow-rate scales with the stellar mass (Peeples and Shankar, 2011; Sanders et al., 2021). The gas expelled is generally more enriched than the average ISM, and outflows are expected to be much more effective in low-mass galaxies with shallower gravitational potential wells (Tremonti et al., 2004). The normalisation of the MZR (whose exact determination is however largely dependent on the assumed method for metallicity determination, see Section 2) reflects instead the asymptotic metallicity value reached in equilibrium conditions, i.e. when the amount of metals produced by massive stars equals the mass of metals locked up in low-mass stars, and is therefore directly related to the nucleosynthetic stellar yields. Finally, in several analytical models the ‘turnover’ mass (i.e. the stellar mass value at which the MZR

begins to flatten-out) is related to the gas fraction in galaxies (Zahid et al., 2014).

Alternative and complementary mechanisms invoked to explain the shape of the gas-phase MZR include on-going accretion of pristine gas (diluting the metal content of the ISM, Lagos et al. 2016) and re-cycling of previously enriched gas from the CGM, the latter more relevant in high-mass systems (Péroux et al., 2020). Moreover, the shape of the high-mass end of the IMF could vary with galaxy mass, introducing a systematic change in the average stellar yields and in the rate of metal enrichment (Vincenzo et al., 2016b). Another possible interpretation of the origin of MZR invokes the so-called ‘downsizing’ scenario of galaxy evolution, in which massive galaxies form earlier and evolve faster (being hence more ‘chemically mature’) compared to low-mass systems: in this sense, the MZR represents therefore an evolutionary sequence (Somerville and Davé, 2015). Finally, recent extensive analysis of large statistical samples of resolved MaNGA galaxies employed machine learning techniques to explore the underlying connection between gas-phase metallicity, stellar mass, and proxies of the galaxy gravitational potential, leading however to contradicting results regarding which physical parameter has to be considered the main driver of the MZR (Baker and Maiolino, 2023; Sánchez-Menguiano et al., 2024).

A relationship between stellar mass and stellar metallicity in galaxies is also observed (e.g. Gallazzi et al., 2005; Zahid et al., 2017), although its shape and normalisation depends on whether the derived stellar metallicities are luminosity-weighted (probing mainly young stellar populations and hence being more similar to the gas-phase MZR) or mass-weighted (reflecting the integrated SFH of galaxies and mainly probing metals locked into older stellar populations). Comparing directly gas-phase and stellar MZR provides useful insights into the role of galactic outflows and possible variations in the IMF (Lian et al., 2018). Furthermore, any offset between the stellar MZR of star-forming and passive systems can be related to the physical processes responsible for quenching star-formation in galaxies. Such a difference is for instance clearly observed in local SDSS galaxies, with passive systems being significantly more enriched than star-forming ones of the same stellar mass (Peng et al., 2015; Trussler et al., 2020). A possible scenario to explain this discrepancy invokes the so-called ‘strangulation’ mechanism of galaxy quenching, in which gas accretion is halted in passive galaxies by either dynamical processes or feedback-heating of the galaxy halo while the metallicity keeps increasing as the available gas reservoir is totally consumed.

4.1.2 The relationship between mass, metallicity, star-formation rate, and gas content

Despite its relative tightness, the scatter in the gas-phase MZR is observed to correlate with different galaxy properties. Observationally, the most relevant dependence is with the current level of star formation, in that galaxies with higher star-formation rates are observed to be more metal depleted, on average, than low star-forming galaxies of the same stellar mass. Such secondary dependence of the MZR on the star-formation rate was initially reported by Ellison et al. (2008), and lately parametrised by Mannucci et al. (2010) into a full, three-dimensional relationship between M_* , SFR, and metallicity often referred to as the ‘Fundamental Metallicity Relation’ (FMR, right-hand panel of Fig. 2). By including the SFR into the framework, the scatter around the MZR is reduced down to a level (~ 0.055 dex) comparable with the typical measurement uncertainties (Mannucci et al., 2010; Salim et al., 2014; Curti et al., 2020b). Several other parametrizations of the FMR have been proposed, as its exact shape depends significantly on both sample selection and methods adopted to measure the three relevant physical quantities (Yates et al., 2012; Andrews and Martini, 2013; Telford et al., 2016; Hunt et al., 2016). Despite some initial contradicting claims (Sánchez et al., 2016; Barrera-Ballesteros et al., 2017), this relationship has been observed to hold also at the local, spatially resolved level probed by integral-field spectroscopic surveys (Cresci et al., 2019), revealing the effect of the interplay of processes occurring on both small scales (e.g. local mass assembly) and global scales (e.g. galaxy-wide outflows) onto the chemical enrichment of individual star-forming regions within galaxies (Barrera-Ballesteros et al., 2016; Baker et al., 2023).

The small amount of scatter around the FMR supports a scenario in which chemical enrichment is regulated by smooth, secular evolutionary processes which set an equilibrium between gas accretion, star-formation, and outflows. Indeed, the existence of the FMR can be explained assuming that star-forming galaxies do most of their growing in a steady-state mode where SFR, metallicity, and gas fraction constantly adjust on a relatively short timescale to reflect the influence of inflows. Cosmological accretion of external gas does not change the stellar mass, but it decreases the mean metallicity of the ISM while simultaneously triggering new star formation episodes. As time goes on, star formation consumes the gas and increases its metallicity, until new metal-poor gas arrives and the cycle starts over. If samples of galaxies with similar M_* are observed at different phases of this cycle (initially triggered by a gas accretion event) they will show a dispersion in metallicity which anti-correlates with the instantaneous SFR, producing the observational signature of the FMR. Theoretical frameworks such as ‘gas-regulator’ models described in the previous section generally predict the existence of the FMR, which arises directly by the assumed balance between the inflow and outflow rates and galaxy internal processes (Davé et al., 2011; Lilly et al., 2013; Dayal et al., 2013). Similarly, an FMR is ‘observed’ also in several cosmological simulations, as driven by the link between gas fraction and SFR (De Rossi et al., 2017; Davé et al., 2017; Torrey et al., 2019) and its exact shape also reflects the detailed prescriptions on the treatment of star-formation and AGN-driven feedback in galaxies (Ma et al., 2016).

As suggested by even the more basic chemical evolution models, both SFR and metallicity are related to the gas reservoir of galaxies, in that higher gas fractions correspond simultaneously to higher SFR and lower metallicities at fixed M_* , and this principle is at the basis of the success of many analytical and numerical prescriptions in matching observations. Therefore, it is not unexpected that such an anti-correlation between metallicity and gas fraction should be directly observed in galaxies and that, moreover, this might be even more ‘fundamental’ (from a physical perspective) than that observed with the SFR. Despite the large observational challenges associated with measuring the gas content in galaxies, both because of the systematics (and metallicity dependence) affecting its tracers or due to its multi-phase nature⁸ (Bolatto et al., 2013; Tacconi et al., 2018), several studies reported possible evidence of an anti-correlation between the gas-phase metallicity and either atomic (Bothwell et al., 2013; Jimmy et al., 2015) or molecular (Bothwell et al., 2016) hydrogen, the latter

⁸hydrogen can be found in either atomic or molecular phase

more directly related to the process of star-formation.

4.1.3 Redshift evolution

To study the evolution of the mass-metallicity relation with redshift is key to constrain the chemical yields of early stellar populations as well as to unveil the role played by gas flows in the regulation of the gas content in galaxies at different epochs and for different mass regimes. Observationally, extensive spectroscopic campaigns have been conducted within the past decades, leveraging in particular the advent, from the early 2000s, of near-infrared multi-object spectrographs on 8-meters class telescopes that allowed to target rest-frame optical metallicity diagnostics in galaxies up to redshift of $z \sim 3$.

Despite the large variety of studied samples and adopted methodologies, a clear picture of the MZR evolution emerged, with high-redshift sources observed to be less enriched than local galaxies of the same stellar mass. Such a decrease in galaxy metallicity with redshift at fixed mass can be ascribed to different mechanisms, including an enhanced gas fraction at high- z from large inflow rates, an increased efficiency in metals removal by star-formation-driven outflows, or a change in the stellar yields, possibly associated with an evolution in the shape of the stellar IMF.

The investigation of the redshift evolution of the MZR is prone to multiple systematics effects, the most relevant being associated with biases in the excitation properties and star-formation rates of the selected samples, uncertainties on the reddening correction, and adoption of different sets of metallicity calibrations and diagnostics. This led to discrepancies among literature studies in the determination of the ‘amplitude’ of the evolution, both in terms of slope and normalisation. While earlier works reported a large evolution, especially at low masses and $z \gtrsim 2$ (e.g. $\sim 0.3 - 0.4$ dex at $M_\star = 10^{10} M_\odot$, Maiolino et al., 2008; Mannucci et al., 2009; Onodera et al., 2016), suggesting a ‘chemical downsizing’ scenario⁹, later studies based on more representative sample of $z \approx 1 - 3$ galaxies, and which adopted a careful and consistent approach in the metallicity determination via strong-line diagnostics, derived a relatively smooth variation in $\log(O/H)$ with redshift at fixed M_\star and no clear evolution in the MZR slope in the ‘intermediate’ mass regime ($9 \leq \log(M_\star / M_\odot) \leq 10.5$) (Sanders et al., 2021; Topping et al., 2021), with this trend now suggested to hold even in the dwarf galaxy regime (Revalski et al., 2024). As the MZR slope reflects the efficacy of stellar winds in removing metals from the ISM, a redshift-invariant MZR slope up to $z \approx 3$ suggests that the physical mechanisms driving outflows in star-forming galaxies remain the same across more than 10 Gyr of cosmic time (Sanders et al., 2021). At the same time, the evolution in the MZR normalisation towards lower O/H at fixed M_\star with increasing redshift can be explained (beside the impact of metal-enriched gas outflows) by the ‘dilution’ effect associated with the larger gas reservoirs of high- z galaxies, in agreement with the observed scaling of both gas content and star-formation efficiency with redshift (Tacconi et al., 2020), as well as with some of the most recent predictions from cosmological simulations based on hierarchical galaxy formation (Davé et al., 2017; Torrey et al., 2019).

When including the SFR into the picture however, hence moving to the framework of the FMR discussed in Section 4.1.2, the situation changes. Remarkably, not only does accounting for the SFR dependence reduce the scatter of the $z \sim 0$ MZR, but high-redshift systems up to $z \sim 2 - 3$ have been observed to obey, on average, the same $z \sim 0$ (e.g. Cresci et al., 2019; Sanders et al., 2021). This suggest that galaxy evolution proceeds as driven by the same interplay between gas flows and internal, secular processes over at least ~ 10 Gyr of cosmic time. Whereas the MZR is observed to evolve with redshift, the FMR concept captures well such scenario, explaining the MZR evolution as a projection effect driven by high- z galaxies preferentially probing different regions of the same, non-evolving FMR at different cosmic epochs (Mannucci et al., 2010). Whether galaxy evolution in the very high-redshift Universe followed similar paths, and how this was reflected into the chemical enrichment properties of galaxies, have been unsolved questions for many years.

4.1.4 The advent of JWST and most recent developments

The advent of the JWST marked the beginning of a new era by opening the long-awaited window onto the properties of high- z galaxies. Rest-frame optical lines previously inaccessible beyond $z \sim 3$ suddenly enabled to characterize the star-formation, metallicity, ionization, and dust properties of thousands of galaxies up to the earliest phases of structure formation. Crucially, the improvement in sensitivity and wavelength coverage in the near-infrared provided by the NIRSpec instrument, coupled with the average decrease in metallicity (and enhancement in ionization) of early galaxy populations, allowed to perform much more robust metallicity measurements in high- z galaxies than ever before, either via direct detections of auroral lines in individual spectra (Curti et al., 2023; Laseter et al., 2023), or exploiting the latter to deliver more reliable diagnostics for the high- z Universe (Sanders et al., 2023).

At the time of writing this Chapter, and after more than two years of JWST operations, the landscape is in rapid evolution. Nonetheless, the scenario depicted by early JWST studies reveals that the MZR is already in place by $z \sim 6 - 8$ over a large range in stellar mass (Nakajima et al., 2023; Curti et al., 2024a; Chemerynska et al., 2024), though with milder evolution in normalization from $z \sim 2 - 3$ than several models would have predicted (e.g. Ucci et al., 2023), suggesting that star-formation and enrichment proceed fast in the early phases of galaxy assembly. Interestingly, indications of a possible flattening of the MZR slope in the low- M_\star regime has been found (Curti et al., 2024a), which would point to a change in the main mechanisms driving galactic outflows and their scaling with stellar mass, favoring ‘momentum-driven’ over ‘energy-driven’ modes.

At the same time, and in tension with past observations out to $z \sim 2 - 3$, a large fraction of high- z galaxies are observed to significantly diverge from the local FMR in that they appear less enriched than its local parametrization would predict for a given M_\star and SFR (Heintz et al., 2023; Nakajima et al., 2023; Curti et al., 2024a). Furthermore, such a deviation appears not as a systematic offset but as a highly scattered distribution. This suggests that, although the global enrichment still reflects the assembled stellar mass (as seen in the MZR), the current

⁹massive galaxies have formed faster, reaching the chemical enrichment level of their local counterparts at earlier epochs

SFR might not capture anymore second-order deviations in the metallicity, and hence the equilibrium between gas flows, star-formation, metal production and outflows that regulate galaxy growth across the latest ~ 10 Gyr of cosmic time might be starting to break-down. To understand whether such an offset can be reconciled by a change of parametrization (hence assuming a redshift-evolving FMR in which the relative strength of the metallicity-SFR dependence at fixed M_* changes with time, e.g. Garcia et al. 2024) or hint at more profound change in the main mode of galaxy assembly, will be a matter of future work.

Theoretically, deviations from the FMR at high- z could reflect different mechanisms in place. On one hand, they could be driven by cosmological processes in the form of a modulation of gas accretion within dark matter halos, possibly inducing an increased stochasticity in the star-formation episodes (Pallottini et al., 2024): this would dilute the ISM on timescales shorter than required by star-formation to enrich it back to the equilibrium level matched to the average galaxy population at lower redshifts, especially in compact systems (Langeroodi and Hjorth, 2023). On the other hand, star-formation stochasticity can reflect ‘internal’ processes associated with SNe-feedback timescales and energetics, which can in turn impact the gas reservoir and the metal content of the ISM (Muratov et al., 2015). Furthermore, the increased merger rate can perturb the gas, driving instabilities which radially mix metals and trigger star-formation (Bustamante, 2017).

In conclusion, it is important to note that early JWST studies might be potentially biased by not properly accounting for the complicated selection functions of the different observing programmes carried-out within the first few cycles of observations, convolved with the target allocation constraints set by the Micro-Shutter-Array (MSA) of NIRSpec employed for multi-object spectroscopy, and that confirmation (or disproof) of these initial results shall await the analysis of more statistically sound and representative galaxy samples, which will certainly be the subject of multiple studies within the next few years.

4.2 Abundance patterns of different elements

The study of relative abundances of different chemical elements, as produced by distinct stellar processes on varying timescales, provides valuable insights into the star-formation history of galaxies. In fact, α -elements like oxygen (O) and neon (Ne) originate from massive stars dying as core-collapse SNe on timescales of a few Myrs, nitrogen (N) and carbon (C) mainly come from low- to intermediate-mass stars (probing tenths to hundreds of Myrs), while Fe-peak elements probe much longer timescales (up to \sim Gyrs) due to the contribution from Type-Ia SNe (Kobayashi et al., 2020). Therefore, the ratio of α -elements to iron (α/Fe) serves as a clock of the star-formation history, in that galaxies showcasing high α/Fe ratios must have formed over short timescales, before Type Ia SNe could significantly enrich the ISM, while conversely lower α/Fe ratios reflect prolonged star formation periods. More in general, abundance patterns of specific elements can reveal the types of stellar progenitors responsible for enriching the ISM, and might even carry the signatures of the enrichment from the first generation of stars, offering insights into the beginning of the cosmic history of metal production.

Detailed studies of chemical abundances in the Milky Way have been performed over the past decades leveraging large, high-resolution spectroscopic surveys in both optical and near-infrared regimes such as APOGEE (Majewski et al., 2017) and GAIA-ESO (Gilmore et al., 2012), forming the basis of the so-called ‘Galactic Archaeology’ and allowing us to obtain a comprehensive overview of the history of the formation of different Galactic components by studying for instance the distribution of stars over the $[\alpha/\text{Fe}]$ versus $[\text{Fe}/\text{H}]$ diagram as a function of both galactocentric distance and height above the Galactic plane (Hayden et al., 2015).

Performing similar studies in extragalactic sources is of course much more complicated. For most galaxies beyond the Local Group, the study of chemical abundances relies on integrated stellar populations; nonetheless, large spectroscopic surveys have provided valuable insights into the chemical composition of nearby galaxies across a wide range of masses and environments. Early studies based on Lick indices identified an enhancement in α/Fe in early-type galaxies compared to stars in the Galactic disk which correlated with stellar velocity dispersion (a proxy for galaxy mass), suggesting that more massive galaxies formed stars earlier and more efficiently over short timescales than their low-mass counterparts (‘downsizing’ scenario, Conroy et al. 2014); remarkably, this is also been observed at higher redshifts ($z \sim 0.7$) from surveys like LEGA-C (Beverage et al., 2021). Cosmological simulations suggest that fast quenching driven by feedback mechanisms (either from SNe or AGN) may effectively shorten star-formation timescales, reproducing the observed α/Fe trends in massive systems (Segers et al., 2016). Direct measurements of $[\alpha/\text{Fe}]$ at even higher redshift are extremely challenging, and the high signal-to-noise on the continuum required to derive stellar metallicities is generally reached only in composite spectra. Nonetheless, studies that attempted to perform a self-consistent analysis of rest-frame UV (rich of stellar features) and rest-optical (rich of nebular features) spectra consistently found indications for an α -enhancement in $z \sim 2 - 3$ star-forming galaxies up to a factor of $\times 3 - 4$ compared to the solar value (Steidel et al., 2016; Cullen et al., 2021), suggesting these galaxies experienced rapid formation timescales ($\sim 0.5 - 1$ Gyr). Such increase in $[\alpha/\text{Fe}]$ (linked to a lower metallicity of the stellar populations) was also deemed responsible for the observed offset in the location of $z \sim 2 - 3$ galaxies on several rest-optical diagnostic diagrams compared to local systems, as driven by the hardening of the stellar radiation field ionizing the gas (Strom et al., 2017a).

In most systems, especially at high-redshift, the study of relative chemical abundances focuses on the gas-phase, leveraging the presence of bright emission lines of different elements in both optical and UV regimes. In particular, the relative abundances of nitrogen-to-oxygen (N/O) and carbon-to-oxygen (C/O) are the among the most studied, in virtue of the different nucleosynthetic paths of the involved species (Figure 3). For instance, in the low-metallicity regime most of the nitrogen has a primary origin and is generated in massive stars, whereas at higher metallicity nitrogen behave like a secondary¹⁰ nucleosynthesis product, since its production becomes dependent on the previous amount of oxygen (and carbon) synthesized in stars via the CNO cycle, hence increasing with increasing oxygen abundance. From the analysis of large spectroscopic surveys it appears that the local galaxy population is distributed over the N/O vs O/H diagram following a plateau in N/O at low-metallicity (representative of the primary production) and a linear correlation at higher O/H, a clear signature of

¹⁰the yield is proportional to the metallicity of the star at birth, in contrast to primary production in which it is instead independent of the initial metallicity

the contribution from secondary production dominating the nitrogen enrichment (Pilyugin et al., 2012). The exact values of plateau, slope of the linear part, and O/H ‘turnover’ depend on the average star-formation efficiency of the analyzed galaxy sample (Berg et al., 2020), as well as on the methodology adopted to derive the nitrogen abundance (whether this is based on the electron temperature method or on strong-line diagnostics such as [NII]/[OII] or [NII]/[SII], Pérez-Montero and Contini 2009). Furthermore, the distribution of galaxies in the N/O vs O/H diagram is also sensitive to gas inflows, which impact the metallicity but not the relative N/O ratio, moving galaxies towards the left, and outflows with differential metal-loading factors (in which oxygen is expelled preferentially by the SN-driven winds compared to nitrogen), which can move galaxies towards the upper-left part of the diagram (Vincenzo et al., 2016a). Some of the involved processes and their impact on the distribution of galaxies onto the N/O vs O/H diagram are summarized in the left-hand panel of Figure 3. The N/O has been observed also to tightly correlate directly with stellar mass (Masters et al., 2016), and a possible three-dimensional relationship between M_* , SFR, and N/O (analogue to the FMR derived for oxygen abundance) has been inferred for local galaxies, suggesting that systems that simultaneously obey both the ‘oxygen-based’ and ‘nitrogen-based’ FMR shall experience the same combination of pristine inflows and metal-loaded outflows throughout their evolution (Hayden-Pawson et al., 2022).

Similarly, the C/O vs O/H diagram provides key constraints on the SFH of galaxies, thanks to the delayed release of carbon compared to α elements. Deriving carbon abundances however is challenging, due to the lack of bright optical lines and the need to resort to UV transitions such as CIII λ 1907, 09 and CIV λ 1548, 51, mainly leveraging sensitive spectroscopy with HST instruments like the Cosmic Origins Spectrograph (COS). In order to minimize the uncertainties on the differential reddening correction between optical and UV regimes, the C/O is best derived by comparing the intensity of CIII λ 1907, 09 to that of the nearby OIII λ 1661, 66 emission, when also the latter is detected (Amorín et al., 2017). In the local Universe, the distribution of galaxies on the C/O vs O/H diagram is characterized by a large dispersion, though with clear similarities to the N/O abundance patterns, showing a low-metallicity plateau while a steep increase at high O/H, mimicking a secondary production process (right-hand panel of Figure 3). This similarity is further supported by the fairly constant observed C/N ratio, suggesting a common enrichment origin for carbon and nitrogen (Berg et al., 2016). Furthermore, the scatter in the C/O vs O/H diagram can be modeled not only by means of variations in the star-formation history (e.g. in terms of number, duration, and delays of bursts) but also including the impact of oxygen-loaded outflows (Berg et al., 2019).

At high-redshift, despite the inherent observational challenges in detecting relatively faint emission lines such as [NII] λ 6584 and CIII λ 1907, 09, evolution in N/O and C/O has been studied by multiple spectroscopic surveys conducted with both space- and ground-based facilities, despite these being limited to probing epochs only up to $z \sim 2 - 3$ before the arrival of JWST. In the N/O vs O/H diagram, it has been observed that $z \sim 2$ galaxies follow trends similar to local galaxies but with larger scatter (Strom et al., 2017b; Hayden-Pawson et al., 2022), possibly reflecting enhanced star formation efficiencies and inflows of pristine gas.

Indications on the evolution of C/O abundance at high- z mostly come from deep investigations of Ly α emitters at $z \sim 2 - 4$ with optical facilities like VLT/X-SHOOTER and VLT/MUSE (e.g. Vanzella et al., 2016; Matthee et al., 2021; Citro et al., 2024), which found an overall consistency in the C/O trend with metallicity as observed in the local Universe. The most interesting results before JWST followed from studying high- z DLA systems in absorption. In fact, multiple studies reported an enhancement in C/O in DLAs at very low metallicity ($12 + \log(\text{O}/\text{H}) < 7.5$) which resembles that observed in some carbon-enhanced metal-poor (CEMP) stars of the Milky Way halo (Cooke et al., 2017; Saccardi et al., 2023), and which are considered, according to models, as some of the best candidate systems polluted by the nucleosynthetic products of so-called Pair Instability Supernovae originating from massive Pop. III stars progenitors (Venditti et al., 2024).

The systematic investigation of chemical abundance patterns within the epoch of Reionization had to await the arrival of JWST. Among its most remarkable results so far, JWST unveiled a population of $z \gtrsim 6$ galaxies with extremely bright UV nitrogen lines (NIV λ 1485, [NIII] λ 1750), associated with an enhanced nitrogen enrichment given their (relatively low) metallicity (e.g. Cameron et al., 2023; Isobe et al., 2023; Topping et al., 2024). Several mechanisms have been proposed to explain such high N/O, including runaway collision of stars in overdense environments (Charbonnel et al., 2023), stellar winds from very massive stars (VMS, $M_* \gtrsim 100M_\odot$, Vink 2024) or even super massive stars (SMS, $M_* \gtrsim 1000M_\odot$, Marques-Chaves et al. 2024), a top-heavy IMF (Curti et al., 2024b) or stochastic star-formation histories with multiple bursts alternated with lulling periods (Kobayashi and Ferrara, 2024). Overall, the high ISM density and star-formation surface densities observed in such compact, nitrogen-enhanced systems suggest these could be progenitors of present day globular clusters (Charbonnel et al., 2023; Schaerer et al., 2024), in virtue of the similar abundance patterns observed in some dwarf stars within local GCs, or even be associated with the formation and presence of early super-massive black holes (Maiolino et al., 2023; Ji et al., 2024; Watanabe et al., 2024). Whether such nitrogen enhancement is common at high-redshift or if these observations are only probing systems experiencing a specific (though short-lasting) phase of their evolution will require future, deeper rest-frame UV spectroscopy of the broader (and less luminous) galaxy population.

In contrast, the vast majority of C/O measurements at $z \gtrsim 6$ delivered by JWST so far report an overall agreement with the distribution of local galaxies at low metallicity, compatible with a recent history of star-formation and a dominant contribution to ISM enrichment driven by core-collapse supernovae. Nonetheless, a notable exception is represented by the galaxy JADES-GS-z12 (D’Eugenio et al., 2023, $z = 12.5$), whose highly enhanced C/O could possibly be modeled as one of the chemical fingerprints of the enrichment from the first generation of PopIII stars.

4.3 Metallicity gradients in galaxies

Beyond integrated measurements of the ‘average’ metallicity, the spatial distribution of metals within galaxies offers further, critical insights into their baryonic and chemical assembly, particularly regarding the impact of gas flows and dynamical processes. Tracking the evolution of metallicity gradients over time is therefore essential for understanding galaxy evolution.

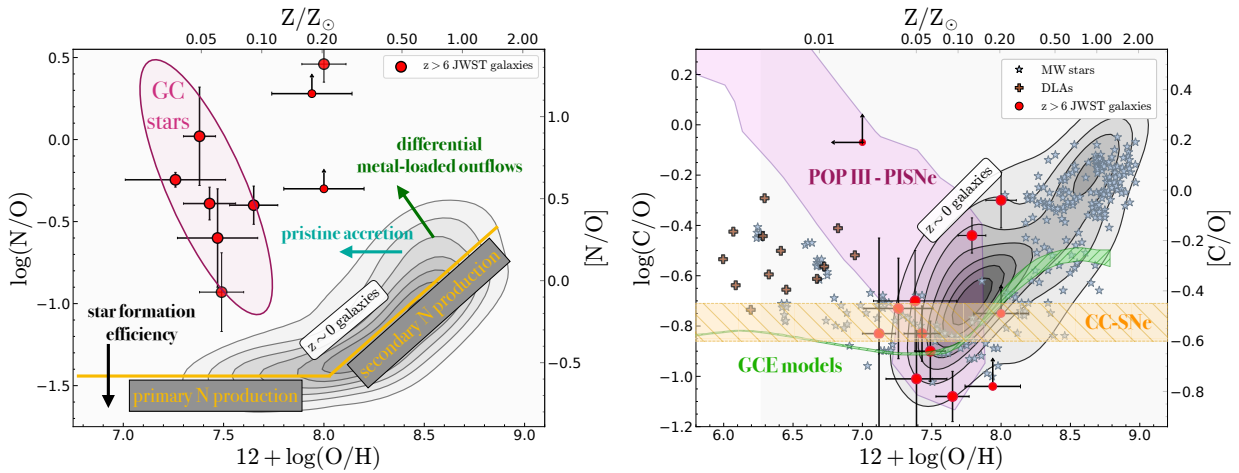


Fig. 3 N/O and C/O abundance ratios as a function of oxygen abundance. The left-hand panel reports the distribution of local $z \sim 0$ galaxies in the N/O vs O/H diagram, highlighting the primary and secondary production sequence and schematizing some of the physical mechanisms that can possibly affect the relationship. The distribution of N-enriched $z > 6$ galaxies observed to date by JWST is also shown: these galaxies showcase super-solar [N/O] and occupy a region of the diagram similar to stars observed within globular clusters in the Milky Way. The right-hand panel reports instead the distribution of Milky Way stars, local galaxies, high-redshift DLAs, and the same JWST sample in the C/O vs O/H diagram. Predictions from pure core-collapse supernovae yields by Tominaga et al. 2007, galactic chemical evolution models of the solar neighborhood from Kobayashi and Taylor (2023), and yields from pair-instability supernovae of Pop III stars progenitors from Vanni et al. (2023) are also shown.

In nearby galaxies, metallicity measurements of individual HII regions reveal a dominance of negative¹¹ metallicity gradients, with central regions more enriched than galaxy outskirts (e.g. Bresolin et al., 2009). This supports the so-called ‘inside-out’ mode of galaxy assembly, where compact cores form early through dissipative processes, whereas disks grow at later times. Theoretical models link these gradients to variations in star formation efficiency, gas fraction, and local enrichment dynamics, influenced by inflows and outflows (e.g. Carton et al., 2015). At large radii ($R > 2R_c$), gradients are often observed to flatten (e.g. Sánchez-Menguiano et al., 2018), likely due to dynamical evolution or the recycling of previously ejected metal-rich gas, a phenomenon known as ‘galactic fountain’ effect (Fraternali, 2017). In interacting galaxies, mergers produce flat gradients due to central inflows of metal-poor gas and mixing processes (e.g. Kewley et al., 2010).

Large statistical studies performed by integral-field spectroscopic surveys such as CALIFA (Sánchez et al., 2012) and MANGA (Bundy et al., 2015) suggest that disk galaxies exhibit a characteristic gradient in oxygen abundance when radial distances are normalised to the galaxy effective radius (Sánchez et al., 2014). This trend initially appeared largely independent of other galaxy properties, suggesting a common evolutionary pathway. However, more statistically sound studies (with samples spanning a wider dynamic range in physical parameters) later suggested instead that the metallicity gradients in star-forming galaxies (even when normalized to R_c) show a clear dependence on stellar mass (Belfiore et al., 2017; Poetrodjojo et al., 2018): gradients are relatively shallow in low-mass galaxies ($M_\star \sim 10^9 M_\odot$), while becoming progressively steeper (more negative) in more massive galaxies. However, gradients seem to flatten-out within the central regions of the most massive systems, likely reflecting the saturation in metallicity as predicted also by many analytical GCE models.

At high redshift, the picture becomes less clear, as a consequence of the increased difficulty of performing spatially resolved metallicity measurements. Although past studies that achieved high spatial resolution (\lesssim kpc-scale) with the aid of adaptive optics, gravitational lensing, and/or by means of slitless spectroscopy with HST, observed steep negative gradients in a few galaxies at $z \gtrsim 1$ (e.g. Jones et al., 2013; Wang et al., 2017), consistent with an ‘inside-out’ growth scenario¹², larger surveys conducted with ground-based telescopes reported a majority of shallow/flat gradients up to $z \sim 2$ (e.g. Stott et al., 2014; Carton et al., 2017; Curti et al., 2020a), suggesting efficient mixing of gas over large scales possibly driven by enhanced feedback mechanisms or merger-driven radial gas flows. Nonetheless, the limited spatial resolution pertaining to seeing-limited observations severely hampers the proper determination of radial trends, and beam-smearing effects can play an important role in biasing and artificially flattening the inferred gradients, especially in low-mass galaxies (Yuan et al., 2013; Wuyts et al., 2016). Remarkably though, a few examples of ‘inverted’, positive gradients (i.e. with central regions of galaxies more metal depleted than the outskirts) have been observed in high- z galaxies, being interpreted as the signature of cold, pristine gas accretion diluting the ISM in the galaxy core (e.g. Cresci et al., 2010; Wang et al., 2019).

Theoretical frameworks, including analytical GCE models and cosmological hydrodynamical simulations, provide predictions for the evolution of metallicity gradients that can be tested with observations. Many models consist in the application of the analytical ‘gas regulator’ prescriptions to concentric galactic rings, in which there is a radial dependence of the main parameters such as the timescale

¹¹The metallicity is generally observed to decrease exponentially with galactocentric radius; therefore, its logarithmic form, $12 + \log(O/H)$, varies linearly with radius

¹²galaxies initially form their central region, producing a steep negative gradient, which then flatten with cosmic time

of gas infall and the star formation efficiency, whereas other models also invoke possible radial variations in the IMF. While these models naturally comply with the ‘inside-out’ growth scenario of mass assembly suggested by colour and stellar population age gradients, they predict much steeper gradients at high- z than in the local Universe (at odd with most observations) unless mechanisms that allow gas and metals to be exchanged radially are implemented. Possible solutions include stellar migration (e.g. Spitoni et al., 2015), prominent radial flows of gas that can dilute the central regions at early epochs (e.g. Mott et al., 2013), or strong feedback that expelled metals produced by central star-formation into the circumgalactic medium and towards the external regions of galactic discs, in line with observations of a relatively enriched CGM at $z \sim 2$ (e.g. Prochaska et al., 2013). Similarly, zoom-in cosmological simulations require to include strong feedback mechanisms (including radiation pressure from massive stars) in order to reproduce shallow metallicity gradients at $z \sim 2$ (e.g. Gibson et al., 2013). Furthermore, the increased scatter in the observed distribution of gradients at high-redshift possibly reflect the increased stochasticity of the star-formation process at earlier cosmic epochs, coupled with the impact of strong feedback associated with starburst episodes (Ma et al., 2017).

Beyond radial trends, azimuthal variations in metallicity (at fixed radius) have been investigated in local spirals, finding evidence for a (small) offset between arm and inter-arm regions (Sánchez-Menguiano et al., 2017; Ho et al., 2018). However, it is important to note that the irregular morphologies, multi-component and ‘clumpy’ nature of many high- z galaxies can make the analysis of radial averages in these systems potentially deceiving. While already suggested in the past by seeing-limited studies (Curti et al., 2020a), this is becoming increasingly evident thanks to recent, higher resolution observations performed with the integral-field spectrograph of JWST/NIRSpec, highlighting the importance of studying the full metallicity distribution and its connection to the star-formation properties and kinematics of each galaxy sub-components in order to get a more comprehensive view of galaxy assembly in the early Universe (e.g. Rodríguez Del Pino et al., 2024; Jones et al., 2024).

4.4 Metals in the circumgalactic medium

Probing the metallicity structure of the circumgalactic medium (CGM) is key to constrain the role of gas flows, cosmic accretion history, and environmental interactions in driving the baryon cycle and its impact onto galaxy evolution. Because of the much lower density and surface brightness of the gas in the CGM compared to the ISM of galaxies, metallicity measurements via detection of line emission are extremely challenging, despite the progress marked over the past years by deep galaxy surveys with IFU instruments like VLT/MUSE (e.g. Dutta et al., 2023). Therefore, the investigation of the metal content of the CGM mostly relies on absorption line techniques as described in Section 2.4. Indeed, most of the information on metals in the CGM comes from absorption lines in the UV region of the spectrum from elements like carbon, nitrogen, oxygen, silicon, iron, magnesium, calcium.

The CGM is a multi-phase medium, constituted by a wide range of density, temperature, and ionization conditions. Simulations reveal structured CGM gas at high redshifts, with accreting gas in filaments and outflows forming biconical patterns (Corlies and Schiminovich, 2016). However, at lower redshifts, the CGM becomes more mixed, and gas velocities provide less insight into its origin (Christensen et al., 2016). In general, absorption spectroscopy using the galaxy’s own starlight as a background source (so-called ‘down-the-barrel’ technique) is capable to distinguish inflows from outflows by interpreting blueshifted absorption as tracing outflowing gas and redshifted absorption as tracing inflowing gas, respectively; it mainly probes gas at the disk-halo interface, but the galactocentric radius of any detected absorption is basically unconstrained. On the other hand, transverse absorption spectroscopy using distant quasars provides a more direct measure of the distance between the galaxy and the probed sightline, but the direction of the gas flow is degenerate such that blueshifted absorption might be related to infalling gas behind the galaxy or equally to outflowing gas in front of the galaxy, and viceversa for redshifted absorption. Combining both observations (when possible) can increase the complexity of the interpretation but also provide deeper insights into the dynamics of the CGM than either alone.

The metal content of galactic flows can serve in principle to distinguish their origin, in that one would expect infalling gas to be nearly-pristine while outflows to be metal-enriched due to star-formation processes taking place inside galaxies (as observationally suggested in the past by the study of a large sample of LLSs revealing a bi-modal metallicity distribution, e.g. Lehner et al., 2013), or to distinguish between systems associated with either the CGM of galaxies or with the IGM (Berg et al., 2023). Gas accreting onto galaxies from the cosmic web passes through the CGM on its journey from the IGM to galaxies, where it leaves observable signatures that can be exploited to trace the inflows (Tumlinson et al., 2017). In this sense, cold, dense, metal-poor CGM gas observed in the form of LLS is considered a strong indicator of cosmological gas accretion at all redshifts, as also predicted by simulations (Hafen et al., 2017).

On the other hand, we have seen that galactic outflows represent a critical component for most galaxy evolution models. Indeed, large-scale outflows have been observed at almost all cosmic epochs (Rupke, 2018), providing feedback that influences the star-formation process in galaxies and carrying metals far from their formation site, possibly into the circumgalactic medium or even beyond (Peroux and Howk, 2020). For instance, observations of widespread OVI around galaxies as detected by COS-Halos surveys confirmed the presence of extended metal-enriched outflows up to ~ 300 kpc (Johnson et al., 2015), and simulations predict that the time-integrated effect of enriched outflows are necessary to produce the observed reservoir of metals (Suresh et al., 2017). Probing the metal enrichment in the CGM is also relevant to constrain the nature of the mechanisms powering outflows in galaxies, discriminating between ‘momentum-driven’ (with velocity scaling as $v \propto v_{\text{circ}}^{-1}$) and ‘energy-driven’ ($v \propto v_{\text{circ}}^{-2}$) winds, which can produce for instance different slopes of the mass-metallicity relation (Finlator and Davé, 2008; Curti et al., 2024a).

Furthermore, it is possible that a substantial fraction of gas accreted onto galaxies has been recycled from previously ejected (and enriched) material, as predicted by several simulations (e.g. Muratov et al., 2017), although the timescales of the process and their dependence on the halo mass are not fully constrained. Recycled accretion might arise from either the ejection of metal-enriched galactic winds lacking the energy to escape the halo, from the same winds losing energy by shocks, mixing into the CGM and then eventually cooling and

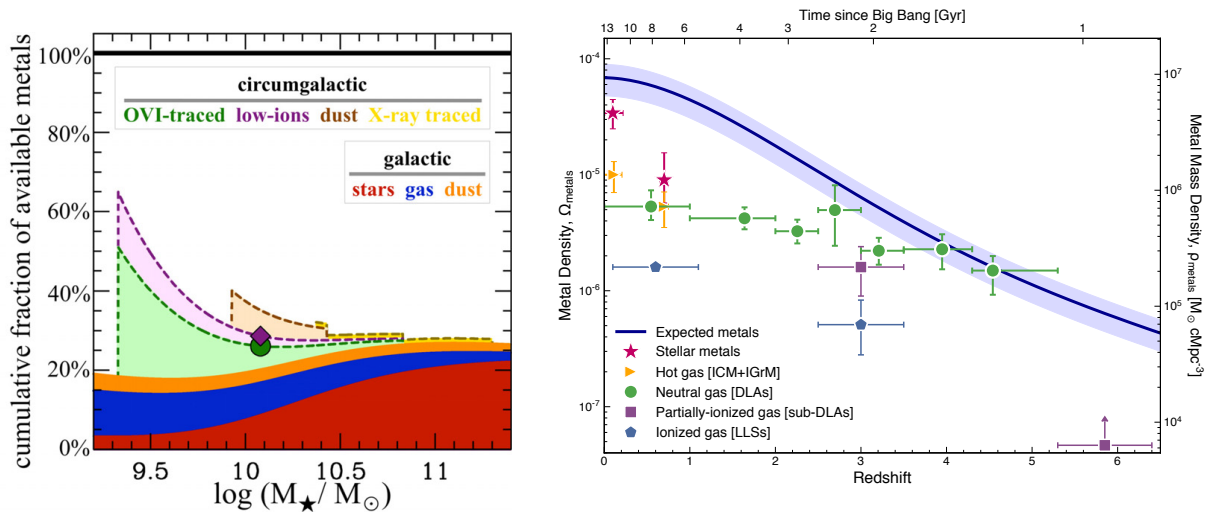


Fig. 4 A census of metals observed in different phases. The left-hand panel reports the cumulative fractions of available metals as a function of stellar mass at $z=0$, whereas the right-hand panel traces the evolution of cosmic metal densities in different components as a function of redshift. Reproduced with permission from Peebles et al. 2014 and Peroux and Howk 2020.

raining back onto the galaxy, or from pristine inflows entraining metal-polluted CGM material on its way from the IGM to the galaxy (e.g. Fraternali, 2017; Tumlinson et al., 2017). Despite being often neglected in the framework of ‘gas-regulator’ chemical evolution models, metal-enriched recycling might therefore constitute an important mechanisms for galaxies to acquire their gas.

4.5 The metal budget

Beside the metallicity (i.e. a relative measurement of the abundance of heavy element compared to hydrogen), accounting for the total mass of metals produced by stars in galaxies over their lifetime and their relative distribution within different components (stars, ISM, dust, CGM, etc..) provides a useful benchmark to test our understanding of the cosmic star-formation history and the role of gas flows in galaxy evolution. These are no less than difficult measurements, as inferring the total content of metals often implies having a good knowledge of the total mass associated with all the involved phases.

Historically, large efforts in this area were triggered by early indications for the observed amount of metals in stars and neutral gas to be significantly lower (about one order of magnitude) than expected based on the integrated star formation rate density evolution of the Universe (Pettini, 1999). This ‘missing metals problem’ has been then re-assessed multiple times ever since, leveraging the increased number of observational constraints spanning a wide range of time in cosmic history. For instance, a full census of metals in galaxies at $z \sim 0$ was performed by Peebles et al. (2014), which found that the amount of metals found in stars, interstellar gas, and interstellar dust (i.e. those retained inside galaxies) represent only 20–30% of the total metal production over three orders of magnitude in stellar mass (modulo the uncertainties on the assumed stellar yields), indicating that galaxies lose the majority of heavy elements they produce (Fig. 4, left panel). Including metals observed in the different phases of the CGM (out to $\sim 150 \text{ kpc}^{13}$) it is possible to account for about half of the metals produced by typical star-forming galaxies. Most of the metals in the CGM are in a highly-ionized phase, traced e.g. by O IV (Tumlinson et al., 2011), or depleted onto dust, whereas the relative contribution of the hot-CGM ($T > 6 \times 10^6 \text{ K}$) gas component is small compared to the ISM phase.

Furthermore, by combining absorption-line derived metal abundances (accounting for dust depletion and ionization corrections) with the cosmological density of the same absorbing systems, it is possible to self-consistently assess the contribution of neutral and ionized gas to the total metal content of the Universe as a function of redshift, and compare it to the total comoving metal mass density produced by stars at each given cosmic epoch. Such a revisited, detailed census has been presented by Peroux and Howk (2020) (see also Yates et al. 2021 for a comparison with predictions from different cosmological simulations), which found that metals in the neutral gas phase dominate over the ionized component and show a mild evolution with redshift (Fig. 4, right panel). At the higher redshifts ($2.5 < z < 5$), the vast majority all of the expected metals are found in the neutral phase (with a relatively significant contribution of ionized absorbers at $z \sim 3$), whereas at lower redshifts ($z \lesssim 1$) the contributions are more diverse, with the stars dominating the metal budget but with also significant contribution from the hot gas within the intracluster medium (ICM) and intragroup medium (IGrM). Although there are still specific redshift ranges that needs to be properly characterized due to intrinsic observational challenges in probing metals in their different phases (and which shall await future X-ray/UV facilities such as ATHENA and LUVOIR, especially for the hot gas component), the ‘missing metals problem’ is therefore largely reduced as of today, and the expected metal content of the Universe is now largely accounted for, once the large uncertainties ($\approx 30\%$) on the assumed stellar yields are considered.

¹³hence sampling different fractions of the virial radius with respect to stellar mass

5 Conclusions and future prospects

In this chapter, we have provided an overview of the key methodologies, observational findings, and their constraints on models that form the foundation of the study of chemical evolution in galaxies across cosmic time. Over the past decade, advancements in ground- and space-based facilities, culminating in the launch of JWST in 2021, have addressed long-standing challenges in the field. These efforts have linked the chemical enrichment properties of galaxies across different spatial and temporal scales, while also delivering surprising results that challenge prior interpretations, offering novel and more robust constraints on models and pushing the boundaries of our understanding.

The future of this field is exceptionally promising, with major progress expected on several interconnected fronts in the coming years. Over the next decade in fact, the investigation of the metal content in galaxies will proceed over parallel, though deeply interconnected, avenues. On the one hand, JWST will continue its groundbreaking exploration of the early universe, unveiling new peculiar systems, constraining enrichment mechanisms, and probing the timescales of chemical evolution in the earliest galaxies. Its expanding datasets will enable more robust statistical study of metallicity scaling relations at high redshift, establishing robust connections between the chemical properties of galaxy populations at different cosmic epochs.

On the other hand, next generations, high-multiplexing, optical multi-object spectrographs on 4-meter class telescopes, such as 4MOST on ESO/VISTA, will deliver millions of high-resolution spectra, spanning ~ 7 billion years of cosmic history. These observations will tightly link the chemical properties of galaxies to their location within the cosmic web, providing unprecedented insights into the relationship between environment and metal enrichment. Similarly, near-infrared spectrographs like PFS on Subaru and MOONS on the VLT will extend these surveys to higher redshifts ($z \sim 1 - 2$), replicating SDSS-like studies at ‘Cosmic Noon’¹⁴ while marking an unprecedented improvement in statistics and completeness at these epochs. These facilities will allow for detailed examinations of environmental effects on metallicity scaling relations (for both gas-phase and stellar metallicities), as well as on quenching mechanisms and their associated timescales by linking the metal content of local passive systems with that of their ‘direct’, high- z star-forming progenitors (e.g. Peng et al., 2015; Trussler et al., 2020).

Finally, within the next decade, the advent of extremely large telescopes (ELTs) will mark a transformative step in galactic chemical evolution studies. The ESO E-ELT, featuring a 39-meter primary mirror, will be the first of its kind and promises to revolutionize multiple areas of research with its unparalleled light-collecting power, cutting-edge instrumentation, and deeply integrated support from adaptive optics. For instance, MICADO will provide both imaging and single-slit NIR spectroscopy, delivering spectra of individual HII regions in $z \sim 1 - 2$ galaxies, while the optical/NIR IFS HARMONI will directly map stellar populations, abundances, and kinematics at 100 pc resolution in $z \sim 2$ galaxies, capturing the most detailed, spatially resolved view of the epoch of the peak of galaxy assembly. Leveraging the huge collecting area of the telescope, MOSAIC will probe metals in the CGM at high- z from absorption spectra using relatively faint galaxies (rather than rare, bright quasars) as background sources, hence increasing the number of observable systems at high spectral resolution by orders of magnitude, while the high-resolution spectrograph ANDES ($R \sim 100,000$) will search for direct signatures (i.e. Hydrogen lines with no metal transitions) of Population III stars, shedding light on the nature of the systems responsible for the synthesis of the first metals in the history of the Universe.

References

- Aller MC, Kulkarni VP, York DG, Welty DE, Vladilo G and Liger N (2014), Apr. Interstellar Silicate Dust in the $z = 0.685$ Absorber Toward TXS 0218+357. *ApJ* 785 (1), 36. doi:10.1088/0004-637X/785/1/36. 1402.4509.
- Amorín R, Fontana A, Pérez-Montero E, Castellano M, Guaita L, Grazian A, Le Fèvre O, Ribeiro B, Schaerer D, Tasca LAM, Thomas R, Bardelli S, Cassarà L, Cassata P, Cimatti A, Contini T, de Barros S, Garilli B, Giavalisco M, Hathi N, Koekemoer A, Le Brun V, Lemaux BC, Maccagni D, Pentericci L, Pforr J, Talia M, Tresse L, Vanzella E, Vergani D, Zamorani G, Zucca E and Merlin E (2017), Mar. Analogues of primeval galaxies two billion years after the Big Bang. *Nature Astronomy* 1: 0052. doi:10.1038/s41550-017-0052.
- Andrews BH and Martini P (2013), Mar. The Mass-Metallicity Relation with the Direct Method on Stacked Spectra of SDSS Galaxies. *ApJ* 765: 140. doi:10.1088/0004-637X/765/2/140.
- Asplund M, Grevesse N, Sauval AJ and Scott P (2009), Sep. The Chemical Composition of the Sun. *ARA&A* 47 (1): 481–522. doi:10.1146/annurev.astro.46.060407.145222. 0909.0948.
- Baker WM and Maiolino R (2023), May. Stellar mass, not dynamical mass nor gravitational potential, drives the mass-metallicity relationship. *MNRAS* 521 (3): 4173–4179. doi:10.1093/mnras/stad802. 2303.08145.
- Baker WM, Maiolino R, Belfiore F, Curti M, Bluck AFL, Lin L, Ellison SL, Thorp M and Pan HA (2023), Feb. The metallicity’s fundamental dependence on both local and global galactic quantities. *MNRAS* 519 (1): 1149–1170. doi:10.1093/mnras/stac3594. 2210.03755.
- Barrera-Ballesteros JK, Heckman TM, Zhu GB, Zakamska NL, Sánchez SF, Law D, Wake D, Green JE, Bizyaev D, Oravetz D, Simmons A, Malanushenko E, Pan K, Roman Lopes A and Lane RR (2016), Dec. Do galaxy global relationships emerge from local ones? The SDSS IV MaNGA surface mass density-metallicity relation. *MNRAS* 463: 2513–2522. doi:10.1093/mnras/stw1984.
- Barrera-Ballesteros JK, Sánchez SF, Heckman T, Blanc GA and The MaNGA Team (2017), Jul. Separate Ways: The Mass-Metallicity Relation Does Not Strongly Correlate with Star Formation Rate in SDSS-IV MaNGA Galaxies. *ApJ* 844: 80. doi:10.3847/1538-4357/aa7aa9.
- Belfiore F, Maiolino R, Tremonti C, Sánchez SF, Bundy K, Bershadsky M, Westfall K, Lin L, Drory N, Boquien M, Thomas D and Brinkmann J (2017), Jul. SDSS IV MaNGA - metallicity and nitrogen abundance gradients in local galaxies. *MNRAS* 469: 151–170. doi:10.1093/mnras/stx789.
- Berg DA, Skillman ED, Henry RBC, Erb DK and Carigi L (2016), Aug. Carbon and Oxygen Abundances in Low Metallicity Dwarf Galaxies. *ApJ* 827: 126. doi:10.3847/0004-637X/827/2/126.
- Berg DA, Erb DK, Henry RBC, Skillman ED and McQuinn KBW (2019), Jan. The Chemical Evolution of Carbon, Nitrogen, and Oxygen in Metal-Poor Dwarf Galaxies. *arXiv e-prints*.

¹⁴the epoch of the peak of the cosmic star-formation rate density, Madau and Dickinson (2014)

- Berg DA, Pogge RW, Skillman ED, Croxall KV, Moustakas J, Rogers NSJ and Sun J (2020), Apr. CHAOS IV: Gas-phase Abundance Trends from the First Four CHAOS Galaxies. *The Astrophysical Journal* 893 (2): 96. ISSN 1538-4357. doi:10.3847/1538-4357/ab7eab. <https://iopscience.iop.org/article/10.3847/1538-4357/ab7eab>.
- Berg MA, Lehner N, Howk JC, O'Meara JM, Schaye J, Straka LA, Cooksey KL, Tripp TM, Prochaska JX, Oppenheimer BD, Johnson SD, Muzahid S, Bordoloi R, Werk JK, Fox AJ, Katz N, Wendt M, Peebles MS, Ribaldo J and Tumlinson J (2023), Feb. The Bimodal Absorption System Imaging Campaign (BASIC). I. A Dual Population of Low-metallicity Absorbers at $z \approx 1$. *ApJ* 944 (1), 101. doi:10.3847/1538-4357/acb047. 2204.13229.
- Beverage AG, Kriek M, Conroy C, Bezanson R, Franx M and van der Wel A (2021), Aug. Elemental Abundances and Ages of $z \approx 0.7$ Quiescent Galaxies on the Mass-Size Plane: Implication for Chemical Enrichment and Star Formation Quenching. *ApJ* 917 (1), L1. doi:10.3847/2041-8213/ac12cd. 2105.12750.
- Bolatto AD, Wolfire M and Leroy AK (2013), Aug. The CO-to-H₂ Conversion Factor. *ARA&A* 51: 207–268. doi:10.1146/annurev-astro-082812-140944.
- Boquien M, Burgarella D, Roehlly Y, Buat V, Ciesla L, Corre D, Inoue AK and Salas H (2019), Feb. CIGALE: a python Code Investigating GALaxy Emission. *A&A* 622, A103. doi:10.1051/0004-6361/201834156. 1811.03094.
- Bothwell MS, Maiolino R, Kennicutt R, Cresci G, Mannucci F, Marconi A and Cicone C (2013), Aug. A fundamental relation between the metallicity, gas content and stellar mass of local galaxies. *MNRAS* 433: 1425–1435. doi:10.1093/mnras/stt817.
- Bothwell MS, Maiolino R, Peng Y, Cicone C, Griffith H and Wagg J (2016), Jan. Molecular gas as the driver of fundamental galactic relations. *MNRAS* 455: 1156–1170. doi:10.1093/mnras/stv2121.
- Bresolin F, Gieren W, Kudritzki RP, Pietrzyński G, Urbaneja MA and Carraro G (2009), Jul. Extragalactic Chemical Abundances: Do H II Regions and Young Stars Tell the Same Story? The Case of the Spiral Galaxy NGC 300. *ApJ* 700: 309–330. doi:10.1088/0004-637X/700/1/309.
- Bresolin F, Kudritzki RP, Urbaneja MA, Gieren W, Ho IT and Pietrzyński G (2016), Oct. Young Stars and Ionized Nebulae in M83: Comparing Chemical Abundances at High Metallicity. *ApJ* 830: 64. doi:10.3847/0004-637X/830/2/64.
- Bundy K, Bershady MA, Law DR, Yan R, Drory N, MacDonald N, Wake DA, Cherinka B, Sánchez-Gallego JR, Weijmans AM, Thomas D, Tremonti C, Masters K, Coccato L, Diamond-Stanic AM, Aragón-Salamanca A, Avila-Reese V, Badenes C, Falcón-Barroso J, Belfiore F, Bizyaev D, Blanc GA, Bland-Hawthorn J, Blanton MR, Brownstein JR, Byler N, Cappellari M, Conroy C, Dutton AA, Emsellem E, Etherington J, Frinchaboy PM, Fu H, Gunn JE, Harding P, Johnston EJ, Kauffmann G, Kinemuchi K, Klaene MA, Knapen JH, Leauthaud A, Li C, Lin L, Maiolino R, Malanushenko V, Malanushenko E, Mao S, Maraston C, McDermid RM, Merrifield MR, Nichol RC, Oravetz D, Pan K, Parejko JK, Sanchez SF, Schlegel D, Simmons A, Steele O, Steinmetz M, Thanjavur K, Thompson BA, Tinker JL, van den Bosch RCE, Westfall KB, Wilkinson D, Wright S, Xiao T and Zhang K (2015), Jan. Overview of the SDSS-IV MaNGA Survey: Mapping nearby Galaxies at Apache Point Observatory. *ApJ* 798: 7. doi:10.1088/0004-637X/798/1/7.
- Bustamante S (2017), Jul., Merger-Induced Metallicity Dilution in Cosmological Galaxy Formation Simulations, The Galaxy Ecosystem. Flow of Baryons through Galaxies, Proceedings of the conference held 24-28 July 2017, Garching. Online at <http://galaxyecosystem.wixsite.com/ecog> and [http://galaxyecosystem.wixsite.com/ecog/\\$j\\$/A/\\$z\\$, id.15, pp. 15](http://galaxyecosystem.wixsite.com/ecog/j/A/z, id.15, pp. 15).
- Byler N, Dalcanton JJ, Conroy C, Johnson BD, Levesque EM and Berg DA (2018), Aug. Stellar and Nebular Diagnostics in the Ultraviolet for Star-forming Galaxies. *ApJ* 863 (1), 14. doi:10.3847/1538-4357/aacd50. 1803.04425.
- Cameron AJ, Katz H, Rey MP and Saxena A (2023), Aug. Nitrogen enhancements 440 Myr after the big bang: supersolar N/O, a tidal disruption event, or a dense stellar cluster in GN-z11? *MNRAS* 523 (3): 3516–3525. doi:10.1093/mnras/stad1579. 2302.10142.
- Cappellari M (2017), Apr. Improving the full spectrum fitting method: accurate convolution with Gauss-Hermite functions. *MNRAS* 466: 798–811. doi:10.1093/mnras/stw3020.
- Carnall AC, McLure RJ, Dunlop JS and Davé R (2018), Nov. Inferring the star formation histories of massive quiescent galaxies with BAGPIPES: evidence for multiple quenching mechanisms. *MNRAS* 480 (4): 4379–4401. doi:10.1093/mnras/sty2169. 1712.04452.
- Carton D, Brinchmann J, Wang J, Bigiel F, Cormier D, van der Hulst T, Józsa GIG, Serra P and Verheijen MAW (2015), Jul. Gas-phase metallicity profiles of the Bluedisk galaxies: Is metallicity in a local star formation regulated equilibrium? *MNRAS* 451: 210–235. doi:10.1093/mnras/stv967.
- Carton D, Brinchmann J, Shirazi M, Contini T, Epinat B, Erroz-Ferrer S, Marino RA, Martinsson TPK, Richard J and Patrício V (2017), Jun. Inferring gas-phase metallicity gradients of galaxies at the seeing limit: a forward modelling approach. *MNRAS* 468: 2140–2163. doi:10.1093/mnras/stx545.
- Charbonnel C, Schaerer D, Prantzos N, Ramírez-Galeano L, Fragos T, Kuruvanthodi A, Marques-Chaves R and Gieles M (2023), May. N-enhancement in GN-z11: First evidence for supermassive stars nucleosynthesis in proto-globular clusters-like conditions at high redshift? *A&A* 673, L7. doi:10.1051/0004-6361/202346410. 2303.07955.
- Chemerynska I, Atek H, Dayal P, Furtak LJ, Feldmann R, Greene JE, Maseda MV, Nanayakkara T, Oesch PA, Labbe I, Bezanson R, Brammer G, Cutler SE, Leja J, Pan R, Price SH, Wang B, Weaver JR and Whitaker KE (2024), Jul. The Extreme Low-mass End of the Mass-Metallicity Relation at $z \approx 7$. *arXiv e-prints*. arXiv:2407.17110doi:10.48550/arXiv.2407.17110. 2407.17110.
- Chen Y, Jones T, Sanders R, Fadda D, Sutter J, Minchin R, Huntzinger E, Senchyna P, Stark D, Spilker J, Weiner B and Roberts-Borsani G (2023), Jul. Accurate oxygen abundance of interstellar gas in Mrk 71 from optical and infrared spectra. *Nature Astronomy* 7: 771–778. doi:10.1038/s41550-023-01953-7. 2304.09898.
- Chevallard J and Charlot S (2016), Oct. Modelling and interpreting spectral energy distributions of galaxies with BEAGLE. *MNRAS* 462 (2): 1415–1443. doi:10.1093/mnras/stw1756. 1603.03037.
- Chieffi A and Limongi M (2004), Jun. Explosive Yields of Massive Stars from $Z = 0$ to $Z = Z_{solar}$. *ApJ* 608 (1): 405–410. doi:10.1086/392523. astro-ph/0402625.
- Christensen CR, Davé R, Governato F, Pontzen A, Brooks A, Munshi F, Quinn T and Wadsley J (2016), Jun. In-N-Out: The Gas Cycle from Dwarfs to Spiral Galaxies. *ApJ* 824 (1), 57. doi:10.3847/0004-637X/824/1/57. 1508.00007.
- Citro A, Berg DA, Erb DK, Auger MW, Becker GD, James BL and Skillman ED (2024), Jul. A Comprehensive Metallicity Analysis of J0332-3557: Establishing a $z \approx 4$ Anchor for Direct Gas Metallicity and C/O Abundance Investigations. *ApJ* 969 (2), 148. doi:10.3847/1538-4357/ad4600. 2305.14414.
- Conroy C (2013), Aug. Modeling the Panchromatic Spectral Energy Distributions of Galaxies. *ARA&A* 51: 393–455. doi:10.1146/annurev-astro-082812-141017.
- Conroy C, Graves GJ and van Dokkum PG (2014), Jan. Early-type Galaxy Archeology: Ages, Abundance Ratios, and Effective Temperatures from Full-spectrum Fitting. *ApJ* 780 (1), 33. doi:10.1088/0004-637X/780/1/33. 1303.6629.
- Cooke RJ, Pettini M and Steidel CC (2017), May. Discovery of the most metal-poor damped Lyman- α system. *MNRAS* 467 (1): 802–811. doi:10.1093/mnras/stx037. 1701.03103.
- Corlies L and Schiminovich D (2016), Aug. Empirically Constrained Predictions for Metal-line Emission from the Circumgalactic Medium. *ApJ* 827 (2), 148. doi:10.3847/0004-637X/827/2/148. 1607.08616.
- Cresci G, Mannucci F, Maiolino R, Marconi A, Gnerucci A and Magrini L (2010), Oct. Gas accretion as the origin of chemical abundance gradients

- in distant galaxies. *Nature* 467: 811–813. doi:10.1038/nature09451.
- Cresci G, Mannucci F and Curti M (2019), Jul. Fundamental metallicity relation in CALIFA, SDSS-IV MaNGA, and high- z galaxies. *A&A* 627, A42. doi:10.1051/0004-6361/201834637. 1811.06015.
- Cullen F, Shapley AE, McLure RJ, Dunlop JS, Sanders RL, Topping MW, Reddy NA, Amorín R, Begley R, Bolzonella M, Calabrò A, Carnall AC, Castellano M, Cimatti A, Cirasuolo M, Cresci G, Fontana A, Fontanot F, Garilli B, Guaita L, Hamadouche M, Hathi NP, Mannucci F, McLeod DJ, Pentericci L, Saxena A, Talia M and Zamorani G (2021), Jul. The NIRVANDELS Survey: a robust detection of α -enhancement in star-forming galaxies at $z \approx 3.4$. *MNRAS* 505 (1): 903–920. doi:10.1093/mnras/stab1340. 2103.06300.
- Curti M, Cresci G, Mannucci F, Marconi A, Maiolino R and Esposito S (2017), Feb. New fully empirical calibrations of strong-line metallicity indicators in star-forming galaxies. *MNRAS* 465: 1384–1400. doi:10.1093/mnras/stw2766.
- Curti M, Maiolino R, Cirasuolo M, Mannucci F, Williams RJ, Auger M, Mercurio A, Hayden-Pawson C, Cresci G, Marconi A, Belfiore F, Cappellari M, Cicone C, Cullen F, Meneghetti M, Ota K, Peng Y, Pettini M, Swinbank M and Troncoso P (2020a), Feb. The KLEVER Survey: Spatially resolved metallicity maps and gradients in a sample of $1.2 < z < 2.5$ lensed galaxies. *Monthly Notices of the Royal Astronomical Society* 492 (1): 821–842. ISSN 0035-8711, 1365-2966. doi:10.1093/mnras/stz3379. ArXiv: 1910.13451, <http://arxiv.org/abs/1910.13451>.
- Curti M, Mannucci F, Cresci G and Maiolino R (2020b), Jan. The mass–metallicity and the fundamental metallicity relation revisited on a fully Te-based abundance scale for galaxies. *Monthly Notices of the Royal Astronomical Society* 491 (1): 944–964. ISSN 0035-8711. doi:10.1093/mnras/stz2910. Publisher: Oxford Academic, <https://academic.oup.com/mnras/article/491/1/944/5638748>.
- Curti M, D'Eugenio F, Carniani S, Maiolino R, Sandles L, Witstok J, Baker WM, Bennett JS, Piotrowska JM, Tacchella S, Charlot S, Nakajima K, Maheson G, Mannucci F, Amiri A, Arribas S, Belfiore F, Bonaventura NR, Bunker AJ, Chevallard J, Cresci G, Curtis-Lake E, Hayden-Pawson C, Jones GC, Kumari N, Laseter I, Looser TJ, Marconi A, Maseda MV, Scholtz J, Smit R, Übler H and Wallace IEB (2023), Jan. The chemical enrichment in the early Universe as probed by JWST via direct metallicity measurements at $z \approx 8$. *MNRAS* 518 (1): 425–438. doi:10.1093/mnras/stac2737. 2207.12375.
- Curti M, Maiolino R, Curtis-Lake E, Chevallard J, Carniani S, D'Eugenio F, Looser TJ, Scholtz J, Charlot S, Cameron A, Übler H, Witstok J, Boyett K, Laseter I, Sandles L, Arribas S, Bunker A, Giardino G, Maseda MV, Rawle T, Rodríguez Del Pino B, Smit R, Willott CJ, Eisenstein DJ, Hausen R, Johnson B, Rieke M, Robertson B, Tacchella S, Williams CC, Willmer C, Baker WM, Bhatawdekar R, Egami E, Helton JM, Ji Z, Kumari N, Perna M, Shivaee I and Sun F (2024a), Apr. JADES: Insights into the low-mass end of the mass-metallicity-SFR relation at $3 \leq z \leq 10$ from deep JWST/NIRSpec spectroscopy. *A&A* 684, A75. doi:10.1051/0004-6361/202346698. 2304.08516.
- Curti M, Witstok J, Jakobsen P, Kobayashi C, Curtis-Lake E, Hainline K, Ji X, D'Eugenio F, Chevallard J, Maiolino R, Scholtz J, Carniani S, Arribas S, Baker WM, Bhatawdekar R, Boyett K, Bunker AJ, Cameron A, Cargile PA, Charlot S, Eisenstein DJ, Ji Z, Johnson BD, Kumari N, Maseda MV, Robertson B, Silcock MS, Tacchella S, Übler H, Venturi G, Willmer CNA and Willott C (2024b), Jul. JADES: The star-formation and chemical enrichment history of a luminous galaxy at $z \approx 9.43$ probed by ultra-deep JWST/NIRSpec spectroscopy. *arXiv e-prints*, arXiv:2407.02575doi:10.48550/arXiv.2407.02575. 2407.02575.
- Davé R, Finlator K and Oppenheimer BD (2011), Sep. Galaxy evolution in cosmological simulations with outflows - II. Metallicities and gas fractions. *MNRAS* 416: 1354–1376. doi:10.1111/j.1365-2966.2011.19132.x.
- Davé R, Rafieferantsoa MH, Thompson RJ and Hopkins PF (2017), May. MUFASA: Galaxy star formation, gas, and metal properties across cosmic time. *MNRAS* 467: 115–132. doi:10.1093/mnras/stx108.
- Dayal P, Ferrara A and Dunlop JS (2013), Apr. The physics of the fundamental metallicity relation. *MNRAS* 430: 2891–2895. doi:10.1093/mnras/stt083.
- De Cia A, Ledoux C, Petitjean P and Savaglio S (2018), Apr. The cosmic evolution of dust-corrected metallicity in the neutral gas. *A&A* 611, A76. doi:10.1051/0004-6361/201731970. 1709.06578.
- De Rossi ME, Bower RG, Font AS, Schaye J and Theuns T (2017), Dec. Galaxy metallicity scaling relations in the EAGLE simulations. *MNRAS* 472: 3354–3377. doi:10.1093/mnras/stx2158.
- Dekel A, Birnboim Y, Engel G, Freundlich J, Goerdt T, Mumcuoglu M, Neistein E, Pichon C, Teyssier R and Zinger E (2009), Jan. Cold streams in early massive hot haloes as the main mode of galaxy formation. *Nature* 457: 451–454. doi:10.1038/nature07648.
- Delahaye F and Pinsonneault MH (2006), Sep. The Solar Heavy-Element Abundances. I. Constraints from Stellar Interiors. *ApJ* 649: 529–540. doi:10.1086/505260.
- D'Eugenio F, Maiolino R, Carniani S, Curtis-Lake E, Witstok J, Chevallard J, Charlot S, Baker WM, Arribas S, Boyett K, Bunker AJ, Curti M, Eisenstein DJ, Hainline K, Ji Z, Johnson BD, Looser TJ, Nakajima K, Nelson E, Rieke M, Robertson B, Scholtz J, Smit R, Venturi G, Tacchella S, Übler H, Willmer CNA and Willott C (2023), Nov. JADES: Carbon enrichment 350 Myr after the Big Bang in a gas-rich galaxy. *arXiv e-prints*, arXiv:2311.09908doi:10.48550/arXiv.2311.09908. 2311.09908.
- Dopita MA, Koratkar AP, Evans IN, Allen M, Bicknell GV, Sutherland RS, Hawley JF and Sadler E (1996), Shock Excitation of LINERs, Eracleous M, Koratkar A, Leitherer C and Ho L, (Eds.), *The Physics of Liners in View of Recent Observations*, Astronomical Society of the Pacific Conference Series, 103, pp. 44.
- Dopita MA, Sutherland RS, Nicholls DC, Kewley LJ and Vogt FPA (2013), Sep. New strong-line abundance diagnostics for H II regions: Effects of k-distributed electron energies and new atomic data. *ApJS* 208: 10. doi:10.1088/0067-0049/208/1/10.
- Dopita MA, Kewley LJ, Sutherland RS and Nicholls DC (2016), Feb. Chemical abundances in high-redshift galaxies: a powerful new emission line diagnostic. *Ap&SS* 361: 61. doi:10.1007/s10509-016-2657-8.
- Dubois Y, Pichon C, Welker C, Le Borgne D, Devriendt J, Laigle C, Codis S, Pogosyan D, Arnouts S, Benabed K, Bertin E, Blaizot J, Bouchet F, Cardoso JF, Colombi S, de Lapparent V, Desjacques V, Gavazzi R, Kassin S, Kimm T, McCracken H, Milliard B, Peirani S, Prunet S, Rouberol S, Silk J, Slyz A, Sousbie T, Teyssier R, Tresse L, Treyer M, Vibert D and Volonteri M (2014), Oct. Dancing in the dark: galactic properties trace spin swings along the cosmic web. *MNRAS* 444 (2): 1453–1468. doi:10.1093/mnras/stu1227. 1402.1165.
- Dutta R, Fossati M, Fumagalli M, Revalski M, Lofthouse EK, Nelson D, Papini G, Rafelski M, Cantalupo S, Arrigoni Battaia F, Dayal P, Longobardi A, Péroux C, Prichard LJ and Prochaska JX (2023), Jun. Metal line emission from galaxy haloes at $z \approx 1$. *MNRAS* 522 (1): 535–558. doi:10.1093/mnras/stad1002. 2302.09087.
- Ellison SL, Patton DR, Simard L and McConnachie AW (2008), Jan. Clues to the Origin of the Mass-Metallicity Relation: Dependence on Star Formation Rate and Galaxy Size. *ApJ* 672: L107. doi:10.1086/527296.
- Ferland GJ, Chatzikos M, Guzmán F, Lykins ML, van Hoof PAM, Williams RJR, Abel NP, Badnell NR, Keenan FP, Porter RL and Stancil PC (2017), Oct. The 2017 Release Cloudy. *Rev. Mexicana Astron. Astrofis.* 53: 385–438. doi:10.48550/arXiv.1705.10877. 1705.10877.
- Finlator K and Davé R (2008), Apr. The origin of the galaxy mass-metallicity relation and implications for galactic outflows. *MNRAS* 385 (4): 2181–2204. doi:10.1111/j.1365-2966.2008.12991.x. 0704.3100.
- Fraternali F (2017), Dec., *Gas Accretion via Condensation and Fountains*, Fox A and Davé R, (Eds.), *Gas Accretion onto Galaxies*, Astrophysics and Space Science Library, 430, pp. 323.
- Gallazzi A, Charlot S, Brinchmann J, White SDM and Tremonti CA (2005), Sep. The ages and metallicities of galaxies in the local universe. *MNRAS* 362: 41–58. doi:10.1111/j.1365-2966.2005.09321.x.

- Garcia AM, Torrey P, Ellison S, Grasha K, Hernquist L, Zovaro HRM, Chen QH, Hemler ZS, Kewley LJ, Nelson EJ and Wright RJ (2024), Jun. Does the fundamental metallicity relation evolve with redshift? I: the correlation between offsets from the mass-metallicity relation and star formation rate. *MNRAS* 531 (1): 1398–1408. doi:10.1093/mnras/stae1252. 2403.08856.
- García-Rojas J and Esteban C (2007), Nov. On the Abundance Discrepancy Problem in H II Regions. *ApJ* 670 (1): 457–470. doi:10.1086/521871.0707.3518.
- Gibson BK, Pilkington K, Brook CB, Stinson GS and Bailin J (2013), Jun. Constraining sub-grid physics with high-redshift spatially-resolved metallicity distributions. *A&A* 554: A47. doi:10.1051/0004-6361/201321239.
- Gilmore G, Randich S, Asplund M, Binney J, Bonifacio P, Drew J, Feltzing S, Ferguson A, Jeffries R, Micela G, Negueruela I, Prusti T, Rix HW, Vallenari A, Alfaro E, Allende-Prieto C, Babusiaux C, Babusiaux C, Bensby T, Blomme R, Bragaglia A, Flaccomio E, François P, Irwin M, Koposov S, Korn A, Lanzafame A, Pancino E, Paunzen E, Recio-Blanco A, Sacco G, Smiljanic R, Van Eck S, Walton N, Aden D, Aerts C, Affer L, Alcalá JM, Altavilla G, Alves J, Antoja T, Arenou F, Argiroffi C, Asensio Ramos A, Bailer-Jones C, Balaguer-Núñez L, Bayo A, Barbuy B, Barisevicius G, Barrado y Navascués D, Battistini C, Bellas Velidis I, Bellazzini M, Belokurov V, Bergemann M, Bertelli G, Biazzo K, Bienayme O, Bland-Hawthorn J, Boeche C, Bonito S, Boudreault S, Bouvier J, Brandao I, Brown A, de Bruijne J, Burleigh M, Caballero J, Caffau E, Calura F, Capuzzo-Dolcetta R, Caramazza M, Carraro G, Casagrande L, Casewell S, Chapman S, Chiappini C, Chorniy Y, Christlieb N, Cignoni M, Cocozza G, Colless M, Collet R, Collins M, Correnti M, Covino E, Crnojevic D, Cropper M, Cunha M, Damiani F, David M, Delgado A, Duffau J, Edvardsson B, Eldridge J, Enke H, Eriksson K, Evans NW, Eyer L, Famaey B, Fellhauer M, Ferreras I, Figueras F, Fiorentino G, Flynn C, Folha D, Franciosini E, Frasca A, Freeman K, Fremat Y, Friel E, Gaensicke B, Gameiro J, Garzon F, Geier S, Geisler D, Caffau E, Gibson B, Gomboc A, Gomez A, Gonzalez-Fernandez C, Gonzalez Hernandez J, Gosset E, Grebel E, Greimel R, Groenewegen M, Grundahl F, Guarcello M, Gustafsson B, Hadrava P, Hatzidimitriou D, Hambly N, Hammersley P, Hansen C, Haywood M, Heber U, Heiter U, Held E, Helmi A, Hensler G, Herrero A, Hill V, Hodgkin S, Huelamo N, Huxor A, Ibata R, Jackson R, de Jong R, Jonker P, Jordan S, Jordi C, Jorissen A, Katz D, Kawata D, Keller S, Kharchenko N, Klement R, Kluttsch A, Knude J, Koch A, Kochukhov O, Kontizas M, Koubzsky P, Lallement R, de Laverny P, van Leeuwen F, Lemasle B, Lewis G, Lind K, Lindstrom HPE, Lobel A, Lopez Santiago J, Lucas P, Ludwig H, Lueftinger T, Magrini L, Maiz Apellaniz J, Maldonado J, Marconi G, Marino A, Martayan C, Martinez-Valpuesta I, Matijevic G, McMahon R, Messina S, Meyer M, Miglio A, Mikolaitis S, Minchev I, Minniti D, Moitinho A, Momany Y, Monaco L, Montalto M, Monteiro MJ, Monier R, Montes D, Mora A, Moraux E, Morel T, Mowlavi N, Mucciarelli A, Munari U, Napiwotzki R, Nardetto N, Naylor T, Naze Y, Nelemans G, Okamoto S, Ortolani S, Pace G, Palla F, Palous J, Parker R, Penarrubia J, Pillitteri I, Piotto G, Posbic H, Prisinzano L, Puzeras E, Quirrenbach A, Ragaini S, Read J, Read M, Reyle C, De Ridder J, Robichon N, Robin A, Roeser S, Romano D, Royer F, Ruchti G, Ruzicka A, Ryan S, Ryde N, Santos N, Sanz Forcada J, Sarro Baro LM, Sbordone L, Schilbach E, Schmeja S, Schnurr O, Schoenrich R, Scholz RD, Seabroke G, Sharma S, De Silva G, Smith M, Solano E, Sordo R, Soubiran C, Sousa S, Spagna A, Steffen M, Steinmetz M, Stelzer B, Stempels E, Taberner H, Tautvaisiene G, Thevenin F, Torra J, Tosi M, Tolstoy E, Turon C, Walker M, Wambsganss J, Worley C, Venn K, Vink J, Wyse R, Zaggia S, Zeilinger W, Zoccali M, Zorec J, Zucker D, Zwitter T and Gaia-ESO Survey Team (2012), Mar. The Gaia-ESO Public Spectroscopic Survey. *The Messenger* 147: 25–31.
- Gutkin J, Charlot S and Bruzual G (2016), Oct. Modelling the nebular emission from primeval to present-day star-forming galaxies. *MNRAS* 462: 1757–1774. doi:10.1093/mnras/stw1716.
- Hafen Z, Faucher-Giguère CA, Anglés-Alcázar D, Kereš D, Feldmann R, Chan TK, Quataert E, Murray N and Hopkins PF (2017), Aug. Low-redshift Lyman limit systems as diagnostics of cosmological inflows and outflows. *MNRAS* 469 (2): 2292–2304. doi:10.1093/mnras/stx952.1608.05712.
- Hayden MR, Bovy J, Holtzman JA, Nidever DL, Bird JC, Weinberg DH, Andrews BH, Majewski SR, Allende Prieto C, Anders F, Beers TC, Bizyaev D, Chiappini C, Cunha K, Frinchaboy P, García-Herrández DA, García Pérez AE, Girardi L, Harding P, Hearty FR, Johnson JA, Mészáros S, Minchev I, O’Connell R, Pan K, Robin AC, Schiavon RP, Schneider DP, Schultheis M, Shetrone M, Skrutskie M, Steinmetz M, Smith V, Wilson JC, Zamora O and Zasowski G (2015), Aug. Chemical Cartography with APOGEE: Metallicity Distribution Functions and the Chemical Structure of the Milky Way Disk. *ApJ* 808 (2), 132. doi:10.1088/0004-637X/808/2/132. 1503.02110.
- Hayden-Pawson C, Curti M, Maiolino R, Cirasuolo M, Belfiore F, Cappellari M, Concas A, Cresci G, Cullen F, Kobayashi C, Mannucci F, Marconi A, Meneghetti M, Mercurio A, Peng Y, Swinbank M and Vincenzo F (2022), May. The KLEVER survey: nitrogen abundances at $z = 2$ and probing the existence of a fundamental nitrogen relation. *MNRAS* 512 (2): 2867–2889. doi:10.1093/mnras/stac584. 2110.00033.
- Heintz KE, Brammer GB, Giménez-Arteaga C, Strait VB, del P. Lagos C, Vijayan AP, Matthee J, Watson D, Mason CA, Hutter A, Toft S, Fynbo JPU and Oesch PA (2023), Dec. Dilution of chemical enrichment in galaxies 600 Myr after the Big Bang. *Nature Astronomy* 7: 1517–1524. doi:10.1038/s41550-023-02078-7. 2212.02890.
- Henriques BMB, Yates RM, Fu J, Guo Q, Kauffmann G, Srisawat C, Thomas PA and White SDM (2020), Feb. L-GALAXIES 2020: Spatially resolved cold gas phases, star formation, and chemical enrichment in galactic discs. *MNRAS* 491 (4): 5795–5814. doi:10.1093/mnras/stz3233.2003.05944.
- Ho IT, Meidt SE, Kudritzki RP, Groves BA, Seibert M, Madore BF, Schinnerer E, Rich JA, Kobayashi C and Kewley LJ (2018), Oct. Azimuthal variations of gas-phase oxygen abundance in NGC 2997. *A&A* 618: A64. doi:10.1051/0004-6361/201833262.
- Hopkins PF, Kereš D, Oñorbe J, Faucher-Giguère CA, Quataert E, Murray N and Bullock JS (2014), Nov. Galaxies on FIRE (Feedback In Realistic Environments): stellar feedback explains cosmologically inefficient star formation. *MNRAS* 445 (1): 581–603. doi:10.1093/mnras/stu1738.1311.2073.
- Hunt L, Dayal P, Magrini L and Ferrara A (2016), Dec. Coevolution of metallicity and star formation in galaxies to $z = 3.7$ - II. A theoretical model. *MNRAS* 463: 2020–2031. doi:10.1093/mnras/stw2091.
- Isobe Y, Ouchi M, Tominaga N, Watanabe K, Nakajima K, Umeda H, Yajima H, Harikane Y, Fukushima H, Xu Y, Ono Y and Zhang Y (2023), Dec. JWST Identification of Extremely Low C/N Galaxies with $[N/O] > r_{sim} 0.5$ at $z = 6-10$ Evidencing the Early CNO-cycle Enrichment and a Connection with Globular Cluster Formation. *ApJ* 959 (2), 100. doi:10.3847/1538-4357/ad09be. 2307.00710.
- Jenkins EB (2009), Aug. A Unified Representation of Gas-Phase Element Depletions in the Interstellar Medium. *ApJ* 700 (2): 1299–1348. doi:10.1088/0004-637X/700/2/1299. 0905.3173.
- Ji X, Übler H, Maiolino R, D’Eugenio F, Arribas S, Bunker AJ, Charlot S, Perna M, Rodríguez Del Pino B, Böker T, Cresci G, Curti M, Kumari N and Lamperti I (2024), Apr. GA-NIFS: An extremely nitrogen-loud and chemically stratified galaxy at $z = 5.55$. *arXiv e-prints*, arXiv:2404.04148doi:10.48550/arXiv.2404.04148. 2404.04148.
- Jimmy, Tran KV, Saintonge A, Accurso G, Brough S and Oliva-Altamirano P (2015), Oct. The Gas Phase Mass Metallicity Relation for Dwarf Galaxies: Dependence on Star Formation Rate and H I Gas Mass. *ApJ* 812: 98. doi:10.1088/0004-637X/812/2/98.
- Johnson SD, Chen HW and Mulchaey JS (2015), Sep. On the origin of excess cool gas in quasar host haloes. *MNRAS* 452 (3): 2553–2565. doi:10.1093/mnras/stv1481. 1505.07838.
- Johnson BD, Leja J, Conroy C and Speagle JS (2021), May. Stellar population inference with prospector. *The Astrophysical Journal Supplement Series* 254 (2): 22. doi:10.3847/1538-4365/abef67. https://dx.doi.org/10.3847/1538-4365/abef67.
- Jones TA, Ellis RS, Schenker MA and Stark DP (2013), Dec. Keck spectroscopy of gravitationally lensed $z = 4$ galaxies: Improved constraints on the escape fraction of ionizing photons. *ApJ* 779: 52. doi:10.1088/0004-637X/779/1/52.

- Jones GC, Bunker AJ, Telikova K, Arribas S, Carniani S, Charlot S, D'Eugenio F, Maiolino R, Perna M, Rodriguez Del Pino B, Ubler H, Willott C, Aravena M, Boker T, Cresci G, Curti M, Herrera-Camus R, Lamperti I, Parlanti E, Perez-Gonzalez PG and Villanueva V (2024), May. GA-NIFS: Witnessing the complex assembly of a massive star-forming system at $z = 5.7$. *arXiv e-prints*, arXiv:2405.12955doi:10.48550/arXiv.2405.12955. 2405.12955.
- Katz H (2022), May. RAMSES-RTZ: non-equilibrium metal chemistry and cooling coupled to on-the-fly radiation hydrodynamics. *MNRAS* 512 (1): 348–365. doi:10.1093/mnras/stac423. 2202.04083.
- Kewley LJ and Dopita MA (2002), Sep. Using Strong Lines to Estimate Abundances in Extragalactic H II Regions and Starburst Galaxies. *ApJ* 562: 35–52. doi:10.1086/341326.
- Kewley LJ and Ellison SL (2008), Jul. Metallicity Calibrations and the Mass-Metallicity Relation for Star-forming Galaxies. *ApJ* 681: 1183–1204. doi:10.1086/587500.
- Kewley LJ, Rupke D, Zahid HJ, Geller MJ and Barton EJ (2010), Sep. Metallicity Gradients and Gas Flows in Galaxy Pairs. *ApJ* 721: L48–L52. doi:10.1088/2041-8205/721/1/L48.
- Kobayashi C and Ferrara A (2024), Feb. Rapid Chemical Enrichment by Intermittent Star Formation in GN-z11. *ApJ* 962 (1), L6. doi:10.3847/2041-8213/ad1de1. 2308.15583.
- Kobayashi C and Taylor P (2023), Feb. Chemo-Dynamical Evolution of Galaxies. *arXiv e-prints*, arXiv:2302.07255doi:10.48550/arXiv.2302.07255. 2302.07255.
- Kobayashi C, Karakas AI and Lugaro M (2020), Sep. The Origin of Elements from Carbon to Uranium. *ApJ* 900 (2), 179. doi:10.3847/1538-4357/abac65. 2008.04660.
- Kobulnicky HA and Kewley LJ (2004), Dec. Metallicities of 0.3%–1.0 Galaxies in the GOODS-North Field. *ApJ* 617: 240–261. doi:10.1086/425299.
- Kreckel K, Egorov OV, Egorova E, Blanc GA, Drory N, Kounkel M, Méndez-Delgado JE, Román-Zúñiga CG, Sánchez SF, Stringfellow GS, Stutz AM, Zari E, Barrera-Ballesteros JK, Bizyaev D, Brownstein JR, Congiu E, Fernández-Trincado JG, García P, Hillenbrand LA, Ibarra-Medel HJ, Jin Y, Johnston EJ, Jones AM, Kim JS, Kollmeier JA, Kong S, Krishnarao D, Kumari N, Li J, Long KS, Mata-Sánchez A, Mejía-Narváez A, Popa SA, Rix HW, Sattler N, Serna J, Singh A, Sánchez-Gallego JR, Wofford A and Wong T (2024), Sep. SDSS-V Local Volume Mapper (LVM): A glimpse into Orion. *A&A* 689, A352. doi:10.1051/0004-6361/202449943. 2405.14943.
- Lagos CdP, Theuns T, Schaye J, Furlong M, Bower RG, Schaller M, Crain RA, Trayford JW and Matthee J (2016), Jul. The Fundamental Plane of star formation in galaxies revealed by the EAGLE hydrodynamical simulations. *MNRAS* 459: 2632–2650. doi:10.1093/mnras/stw717.
- Langeroodi D and Hjorth J (2023), Jul. Ultraviolet Compactness of High-Redshift Galaxies as a Tracer of Early-Stage Gas Infall, Stochastic Star Formation, and Offset from the Fundamental Metallicity Relation. *arXiv e-prints*, arXiv:2307.06336doi:10.48550/arXiv.2307.06336. 2307.06336.
- Laseter IH, Maseda MV, Curti M, Maiolino R, D'Eugenio F, Cameron AJ, Looser TJ, Arribas S, Baker WM, Bhatwadekar R, Boyett K, Bunker AJ, Carniani S, Charlot S, Chevallard J, Curtis-lake E, Egami E, Eisenstein DJ, Hainline K, Hausen R, Ji Z, Kumari N, Perna M, Rawle T, Rix HW, Robertson B, Rodríguez Del Pino B, Sandles L, Scholtz J, Smit R, Tacchella S, Übler H, Williams CC, Willott C and Witstok J (2023), Jun. JADES: Detecting [OIII] λ 4363 Emitters and Testing Strong Line Calibrations in the High- z Universe with Ultra-deep JWST/NIRSpec Spectroscopy up to $z \approx 9.5$. *arXiv e-prints*, arXiv:2306.03120doi:10.48550/arXiv.2306.03120. 2306.03120.
- Lee H, Skillman ED, Cannon JM, Jackson DC, Gehrz RD, Polonski EF and Woodward CE (2006), Aug. On Extending the Mass-Metallicity Relation of Galaxies by 2.5 Decades in Stellar Mass. *ApJ* 647: 970–983. doi:10.1086/505573.
- Lehner N, Howk JC, Tripp TM, Tumlinson J, Prochaska JX, O'Meara JM, Thom C, Werk JK, Fox AJ and Ribaldo J (2013), Jun. The Bimodal Metallicity Distribution of the Cool Circumgalactic Medium at $z \approx 1$. *ApJ* 770 (2), 138. doi:10.1088/0004-637X/770/2/138. 1302.5424.
- Leitherer C, Tremonti CA, Heckman TM and Calzetti D (2011), Feb. An Ultraviolet Spectroscopic Atlas of Local Starbursts and Star-forming Galaxies: The Legacy of FOS and GHRS. *AJ* 141 (2), 37. doi:10.1088/0004-6256/141/2/37. 1011.0385.
- Lequeux J, Peimbert M, Rayo JF, Serrano A and Torres-Peimbert S (1979), Dec. Chemical composition and evolution of irregular and blue compact galaxies. *A&A* 80: 155–166.
- Lian J, Thomas D, Maraston C, Goddard D, Comparat J, Gonzalez-Perez V and Ventura P (2018), Feb. The mass-metallicity relations for gas and stars in star-forming galaxies: strong outflow versus variable IMF. *MNRAS* 474: 1143–1164. doi:10.1093/mnras/stx2829.
- Lilly SJ, Carollo CM, Pipino A, Renzini A and Peng Y (2013), Aug. Gas Regulation of Galaxies: The Evolution of the Cosmic Specific Star Formation Rate, the Metallicity-Mass-Star-formation Rate Relation, and the Stellar Content of Halos. *ApJ* 772: 119. doi:10.1088/0004-637X/772/2/119.
- Lofthouse EK, Fumagalli M, Fossati M, O'Meara JM, Murphy MT, Christensen L, Prochaska JX, Cantalupo S, Bielby RM, Cooke RJ, Lusso E and Morris SL (2020), Jan. MUSE Analysis of Gas around Galaxies (MAGG) - I: Survey design and the environment of a near pristine gas cloud at $z \approx 3.5$. *MNRAS* 491 (2): 2057–2074. doi:10.1093/mnras/stz3066. 1910.13458.
- Ma X, Hopkins PF, Faucher-Giguère CA, Zolman N, Muratov AL, Kereš D and Quataert E (2016), Feb. The origin and evolution of the galaxy mass-metallicity relation. *MNRAS* 456: 2140–2156. doi:10.1093/mnras/stv2659.
- Ma X, Hopkins PF, Feldmann R, Torrey P, Faucher-Giguère CA and Kereš D (2017), Apr. Why do high-redshift galaxies show diverse gas-phase metallicity gradients? *MNRAS* 466: 4780–4794. doi:10.1093/mnras/stx034.
- Madau P and Dickinson M (2014), Aug. Cosmic Star-Formation History. *ARA&A* 52: 415–486. doi:10.1146/annurev-astro-081811-125615.
- Maiolino R and Mannucci F (2019), Feb. De re metallica: the cosmic chemical evolution of galaxies. *A&A Rev.* 27: 3. doi:10.1007/s00159-018-0112-2.
- Maiolino R, Nagao T, Grazian A, Cocchia F, Marconi A, Mannucci F, Cimatti A, Pipino A, Ballero S, Calura F, Chiappini C, Fontana A, Granato GL, Matteucci F, Pastorini G, Pentericci L, Risaliti G, Salvati M and Silva L (2008), Sep. AMAZE. I. The evolution of the mass-metallicity relation at $z \approx 3$. *A&A* 488: 463–479. doi:10.1051/0004-6361:200809678.
- Maiolino R, Scholtz J, Witstok J, Carniani S, D'Eugenio F, de Graaff A, Uebler H, Tacchella S, Curtis-Lake E, Arribas S, Bunker A, Charlot S, Chevallard J, Curti M, Looser TJ, Maseda MV, Rawle T, Rodríguez Del Pino B, Willott CJ, Egami E, Eisenstein D, Hainline K, Robertson B, Williams CC, Willmer CNA, Baker WM, Boyett K, DeCoursey C, Fabian AC, Helton JM, Ji Z, Jones GC, Kumari N, Laporte N, Nelson E, Perna M, Sandles L, Shivaiei I and Sun F (2023), May. A small and vigorous black hole in the early Universe. *arXiv e-prints*, arXiv:2305.12492doi:10.48550/arXiv.2305.12492. 2305.12492.
- Majewski SR, Schiavon RP, Frinchaboy PM, Allende Prieto C, Barkhouser R, Bizyaev D, Blank B, Brunner S, Burton A, Carrera R, Chojnowski SD, Cunha K, Epstein C, Fitzgerald G, García Pérez AE, Hearty FR, Henderson C, Holtzman JA, Johnson JA, Lam CR, Lawler JE, Maseman P, Mészáros S, Nelson M, Nguyen DC, Nidever DL, Pinsonneault M, Shetrone M, Smees S, Smith VV, Stolberg T, Skrutskie MF, Walker E, Wilson JC, Zasowski G, Anders F, Basu S, Beland S, Blanton MR, Bovy J, Brownstein JR, Carlberg J, Chaplin W, Chiappini C, Eisenstein DJ, Elsworth Y, Feuillet D, Fleming SW, Galbraith-Frew J, García RA, García-Hernández DA, Gillespie BA, Girardi L, Gunn JE, Hasselquist S, Hayden MR, Hekker S, Ivans I, Kinemuchi K, Klaene M, Mahadevan S, Mathur S, Mosser B, Muna D, Munn JA, Nichol RC, O'Connell RW, Parejko JK, Robin AC, Rocha-Pinto H, Schultheis M, Serenelli AM, Shane N, Silva Aguirre V, Sobek JS, Thompson B, Troup NW, Weinberg DH and Zamora O (2017), Sep. The Apache Point Observatory Galactic Evolution Experiment (APOGEE). *AJ* 154 (3), 94. doi:

- 10.3847/1538-3881/aa784d. 1509.05420.
- Mannucci F, Cresci G, Maiolino R, Marconi A, Pastorini G, Pozzetti L, Gnerucci A, Risaliti G, Schneider R, Lehnert M and Salvati M (2009), Oct. LSD: Lyman-break galaxies Stellar populations and Dynamics - I. Mass, metallicity and gas at $z \sim 3.1$. *MNRAS* 398: 1915–1931. doi:10.1111/j.1365-2966.2009.15185.x.
- Mannucci F, Cresci G, Maiolino R, Marconi A and Gnerucci A (2010), Nov. A fundamental relation between mass, star formation rate and metallicity in local and high-redshift galaxies. *MNRAS* 408: 2115–2127. doi:10.1111/j.1365-2966.2010.17291.x.
- Marques-Chaves R, Schaerer D, Kuruvanthodi A, Korber D, Prantzos N, Charbonnel C, Weibel A, Izotov YI, Messa M, Brammer G, Dessauges-Zavadsky M and Oesch P (2024), Jan. Extreme N-emitters at high redshift: Possible signatures of supermassive stars and globular cluster or black hole formation in action. *A&A* 681, A30. doi:10.1051/0004-6361/202347411. 2307.04234.
- Martin DC, O'Sullivan D, Matuszewski M, Hamden E, Dekel A, Lapiner S, Morrissey P, Neill JD, Cantalupo S, Prochaska JX, Steidel C, Trainor R, Moore A, Ceverino D, Primack J and Rizzi L (2019), Jul. Multi-filament gas inflows fuelling young star-forming galaxies. *Nature Astronomy* 3: 822–831. doi:10.1038/s41550-019-0791-2. 1904.11465.
- Masters D, Faisst A and Capak P (2016), Aug. A TIGHT RELATION BETWEEN N/O RATIO AND GALAXY STELLAR MASS CAN EXPLAIN THE EVOLUTION OF STRONG EMISSION LINE RATIOS WITH REDSHIFT. *The Astrophysical Journal* 828 (1): 18. ISSN 1538-4357. doi:10.3847/0004-637X/828/1/18. <https://iopscience.iop.org/article/10.3847/0004-637X/828/1/18>.
- Matthee J, Sobral D, Hayes M, Pezzulli G, Gronke M, Schaerer D, Naidu RP, Röttgering H, Calhau J, Paulino-Afonso A, Santos S and Amorín R (2021), Jul. The X-SHOOTER Lyman α survey at $z = 2$ (XLS-z2) I: what makes a galaxy a Lyman α emitter? *MNRAS* 505 (1): 1382–1412. doi:10.1093/mnras/stab1304. 2102.07779.
- McGaugh SS (1991), Oct. H II region abundances - Model oxygen line ratios. *ApJ* 380: 140–150. doi:10.1086/170569.
- Méndez-Delgado JE, Esteban C, García-Rojas J, Arellano-Córdova KZ, Kreckel K, Gómez-Llanos V, Egorov OV, Peimbert M and Orte-García M (2023a), Aug. Density biases and temperature relations for DESIRED H II regions. *MNRAS* 523 (2): 2952–2973. doi:10.1093/mnras/stad1569. 2305.13136.
- Méndez-Delgado JE, Esteban C, García-Rojas J, Kreckel K and Peimbert M (2023b), Jun. Temperature inhomogeneities cause the abundance discrepancy in H II regions. *Nature* 618 (7964): 249–251. doi:10.1038/s41586-023-05956-2. 2305.11578.
- Mott A, Spitoni E and Matteucci F (2013), Nov. Abundance gradients in spiral discs: is the gradient inversion at high redshift real? *MNRAS* 435: 2918–2930. doi:10.1093/mnras/stt1495.
- Muratov AL, Kereš D, Faucher-Giguère CA, Hopkins PF, Quataert E and Murray N (2015), Dec. Gusty, gaseous flows of FIRE: galactic winds in cosmological simulations with explicit stellar feedback. *MNRAS* 454 (3): 2691–2713. doi:10.1093/mnras/stv2126. 1501.03155.
- Muratov AL, Kereš D, Faucher-Giguère CA, Hopkins PF, Ma X, Anglés-Alcázar D, Chan TK, Torrey P, Hafen ZH, Quataert E and Murray N (2017), Jul. Metal flows of the circumgalactic medium, and the metal budget in galactic haloes. *MNRAS* 468 (4): 4170–4188. doi:10.1093/mnras/stx667. 1606.09252.
- Nagao T, Maiolino R and Marconi A (2006), Nov. Gas metallicity diagnostics in star-forming galaxies. *A&A* 459: 85–101. doi:10.1051/0004-6361:20065216.
- Nakajima K, Ouchi M, Isole Y, Harikane Y, Zhang Y, Ono Y, Umeda H and Oguri M (2023), Dec. JWST Census for the Mass-Metallicity Star Formation Relations at $z = 4-10$ with Self-consistent Flux Calibration and Proper Metallicity Calibrators. *ApJS* 269 (2), 33. doi:10.3847/1538-4365/acd556. 2301.12825.
- Nelson D, Springel V, Pillepich A, Rodriguez-Gomez V, Torrey P, Genel S, Vogelsberger M, Pakmor R, Marinacci F, Weinberger R, Kelley L, Lovell M, Diemer B and Hernquist L (2019), May. The IllustrisTNG simulations: public data release. *Computational Astrophysics and Cosmology* 6 (1), 2. doi:10.1186/s40668-019-0028-x. 1812.05609.
- Nicholls DC, Sutherland RS, Dopita MA, Kewley LJ and Groves BA (2017), Apr. Abundance scaling in stars, nebulae and galaxies. *MNRAS* 466: 4403–4422. doi:10.1093/mnras/stw3235.
- Onodera M, Carollo CM, Lilly S, Renzini A, Arimoto N, Capak P, Daddi E, Scoville N, Tacchella S, Tatehara S and Zamorani G (2016), May. ISM Excitation and Metallicity of Star-forming Galaxies at $z \sim 3.3$ from Near-IR Spectroscopy. *ApJ* 822: 42. doi:10.3847/0004-637X/822/1/42.
- Pagel BEJ, Edmunds MG, Blackwell DE, Chun MS and Smith G (1979), Oct. On the composition of H II regions in southern galaxies. I - NGC 300 and 1365. *MNRAS* 189: 95–113.
- Pallottini A, Ferrara A, Gallerani S, Vallini L, Maiolino R and Salvadori S (2017), Mar. Zooming on the internal structure of $z \sim 6$ galaxies. *MNRAS* 465: 2540–2558. doi:10.1093/mnras/stw2847.
- Pallottini A, Ferrara A, Gallerani S, Sommovigo L, Carniani S, Vallini L, Kohandel M and Venturi G (2024), Jul. The mass-metallicity relation as a ruler for galaxy evolution: insights from the James Webb Space Telescope. *arXiv e-prints*, arXiv:2408.00061 doi:10.48550/arXiv.2408.00061. 2408.00061.
- Peebles MS and Shankar F (2011), Nov. Constraints on star formation driven galaxy winds from the mass-metallicity relation at $z = 0$. *MNRAS* 417 (4): 2962–2981. doi:10.1111/j.1365-2966.2011.19456.x. 1007.3743.
- Peebles MS, Werk JK, Tumlinson J, Oppenheimer BD, Prochaska JX, Katz N and Weinberg DH (2014), May. A Budget and Accounting of Metals at $z = 0$: Results from the COS-Halos Survey. *ApJ* 786 (1), 54. doi:10.1088/0004-637X/786/1/54. 1310.2253.
- Peimbert M (1967), Dec. Temperature Determinations of H II Regions. *ApJ* 150: 825. doi:10.1086/149385.
- Peimbert M and Peimbert A (2014), Oct., Densities, Temperatures, Pressures, and Abundances Derived from O II Recombination Lines in H II Regions and their Implications, *Revista Mexicana de Astronomía y Astrofísica Conference Series*, *Revista Mexicana de Astronomía y Astrofísica Conference Series*, 44, 137–137.
- Peimbert M, Peimbert A and Delgado-Inglada G (2017), Aug. Nebular Spectroscopy: A Guide on H II Regions and Planetary Nebulae. *PASP* 129 (978): 082001. doi:10.1088/1538-3873/aa72c3. 1705.06323.
- Peng Y, Maiolino R and Cochrane R (2015), May. Strangulation as the primary mechanism for shutting down star formation in galaxies. *Nature* 521: 192–195. doi:10.1038/nature14439.
- Peroux C and Howk JC (2020), Aug. The Cosmic Baryon and Metal Cycles. *ARA&A* 58: 363–406. doi:10.1146/annurev-astro-021820-120014. 2011.01935.
- Péroux C, Nelson D, van de Voort F, Pillepich A, Marinacci F, Vogelsberger M and Hernquist L (2020), Dec. Predictions for the angular dependence of gas mass flow rate and metallicity in the circumgalactic medium. *MNRAS* 499 (2): 2462–2473. doi:10.1093/mnras/staa2888. 2009.07809.
- Pettini M (1999), Jan., Element Abundances at High Redshifts, Walsh JR and Rosa MR, (Eds.), *Chemical Evolution from Zero to High Redshift*, pp. 233, astro-ph/9902173.
- Pettini M (2004), Jan., Element abundances through the cosmic ages, Esteban C, García López R, Herrero A and Sánchez F, (Eds.), *Cosmochemistry. The melting pot of the elements*, 257–298, astro-ph/0303272.
- Pettini M and Pagel BEJ (2004), Mar. [OIII]/[NII] as an abundance indicator at high redshift. *MNRAS* 348: L59–L63. doi:10.1111/j.1365-2966.2004.07591.x.

- Pettini M, Smith LJ, King DL and Hunstead RW (1997), Sep. The Metallicity of High-Redshift Galaxies: The Abundance of Zinc in 34 Damped Ly α Systems from $z = 0.7$ to 3.4 . *ApJ* 486 (2): 665–680. doi:10.1086/304564. astro-ph/9704102.
- Pilyugin LS, Vílchez JM, Cedrés B and Thuan TX (2010), Apr. The electron temperatures of SDSS high-metallicity giant extragalactic HII regions. *MNRAS* 403: 896–905. doi:10.1111/j.1365-2966.2009.16166.x.
- Pilyugin LS, Vílchez JM, Mattsson L and Thuan TX (2012), Apr. Abundance determination from global emission-line SDSS spectra: exploring objects with high N/O ratios. *MNRAS* 421: 1624–1634. doi:10.1111/j.1365-2966.2012.20420.x.
- Poetrodjojo HM, Groves B, Kewley LJ, Medling AM, Sweet SM, Sande Jvd, Sanchez SF, Bland-Hawthorn J, Brough S, Bryant JJ, Cortese L, Croom SM, López-Sánchez AR, Richards SN, Zafar T, Lawrence JS, Lorente NPF, Owers MS and Scott N (2018), Jul. The SAMI Galaxy Survey: Spatially Resolved Metallicity and Ionization Mapping. *MNRAS* doi:10.1093/mnras/sty1782.
- Poudel S, Kulkarni VP, Morrison S, Péroux C, Som D, Rahmani H and Quiret S (2018), Jan. Early metal enrichment of gas-rich galaxies at $z = 5$. *MNRAS* 473 (3): 3559–3572. doi:10.1093/mnras/stx2607. 1710.03315.
- Prochaska JX, Hennawi JF and Simcoe RA (2013), Jan. A Substantial Mass of Cool, Metal-enriched Gas Surrounding the Progenitors of Modern-day Ellipticals. *ApJ* 762 (2), L19. doi:10.1088/2041-8205/762/2/L19. 1211.6131.
- Pérez-Montero E and Contini T (2009), Sep. The impact of the nitrogen-to-oxygen ratio on ionized nebula diagnostics based on [NII] emission lines. *MNRAS* 398: 949–960. doi:10.1111/j.1365-2966.2009.15145.x.
- Revalski M, Rafelski M, Henry A, Fossati M, Fumagalli M, Dutta R, Pirzkal N, Beckett A, Arrigoni Battaia F, Dayal P, D’Odorico V, Lusso E, Nedkova KV, Prichard LJ, Papovich C and Peroux C (2024), Mar. The MUSE Ultra Deep Field (MUDF). V. Characterizing the Mass-Metallicity Relation for Low Mass Galaxies at $z = 1-2$. *arXiv e-prints*, arXiv:2403.17047doi:10.48550/arXiv.2403.17047. 2403.17047.
- Rodríguez Del Pino B, Perna M, Arribas S, D’Eugenio F, Lamperti I, Pérez-González PG, Übler H, Bunker A, Carniani S, Charlot S, Maiolino R, Willott CJ, Böker T, Chevallard J, Cresci G, Curti M, Jones GC, Parlanti E, Scholtz J and Venturi G (2024), Apr. GA-NIFS: Co-evolution within a highly star-forming galaxy group at $z = 3.7$ witnessed by JWST/NIRSpec IFS. *A&A* 684, A187. doi:10.1051/0004-6361/202348057. 2309.14431.
- Rupke DSN (2018), Dec. A Review of Recent Observations of Galactic Winds Driven by Star Formation. *Galaxies* 6 (4), 138. doi:10.3390/galaxies6040138. 1812.05184.
- Saccardi A, Salvadori S, D’Odorico V, Cupani G, Fumagalli M, Berg TAM, Becker GD, Ellison S and Lopez S (2023), May. Evidence of First Stars-enriched Gas in High-redshift Absorbers. *ApJ* 948 (1), 35. doi:10.3847/1538-4357/acc39f. 2305.02346.
- Salim S, Lee JC, Ly C, Brinchmann J, Davé R, Dickinson M, Salzer JJ and Charlot S (2014), Dec. A Critical Look at the Mass-Metallicity-Star Formation Rate Relation in the Local Universe. I. An Improved Analysis Framework and Confounding Systematics. *ApJ* 797: 126. doi:10.1088/0004-637X/797/2/126.
- Sánchez-Menguiano L, Sánchez Almeida J, Sánchez SF and Muñoz-Tuñón C (2024), Jan. Stellar mass is not the best predictor of galaxy metallicity. The gravitational potential-metallicity relation ΦZR . *A&A* 681, A121. doi:10.1051/0004-6361/202346708. 2312.02046.
- Sanders RL, Shapley AE, Jones T, Reddy NA, Kriek M, Siana B, Coil AL, Mobasher B, Shivaei I, Davé R, Azadi M, Price SH, Leung G, Freeman WR, Fetherolf T, de Groot L, Zick T and Barro G (2021), Jun. The MOSDEF Survey: The Evolution of the Mass-Metallicity Relation from $z = 0$ to $z = 3.3$. *ApJ* 914 (1), 19. doi:10.3847/1538-4357/abf4c1. 2009.07292.
- Sanders RL, Shapley AE, Topping MW, Reddy NA and Brammer GB (2023), Mar. Direct T_e-based Metallicities of $z=2-9$ Galaxies with JWST/NIRSpec: Empirical Metallicity Calibrations Applicable from Reionization to Cosmic Noon. *arXiv e-prints*, arXiv:2303.081492303.08149.
- Schaerer D, Marques-Chaves R, Xiao M and Korber D (2024), Jun. Discovery of a new N-emitter in the epoch of reionization. *arXiv e-prints*, arXiv:2406.08408doi:10.48550/arXiv.2406.08408. 2406.08408.
- Schaye J, Crain RA, Bower RG, Furlong M, Schaller M, Theuns T, Dalla Vecchia C, Frenk CS, McCarthy IG, Helly JC, Jenkins A, Rosas-Guevara YM, White SDM, Baes M, Booth CM, Camps P, Navarro JF, Qu Y, Rahmati A, Sawala T, Thomas PA and Trayford J (2015), Jan. The EAGLE project: simulating the evolution and assembly of galaxies and their environments. *MNRAS* 446 (1): 521–554. doi:10.1093/mnras/stu2058. 1407.7040.
- Scholte D, Saintonge A, Moustakas J, Catinella B, Zou H, Dey B, Aguilar J, Ahlen S, Anand A, Blum R, Brooks D, Circosta C, Claybaugh T, de la Macorra A, Doel P, Font-Ribera A, Förster PU, Forero-Romero JE, Gaztañaga E, Gontcho A Gontcho S, Juneau S, Kehoe R, Kisner T, Kopusov SE, Kremin A, Lambert A, Landriau M, Maraston C, Martini P, Meisner A, Mighty AS, Miquel R, Myers AD, Nie J, Poppett C, Prada F, Rezaie M, Rossi G, Sanchez E, Schubnell M, Silber J, Sprayberry D, Siudek M, Speranza F, Tarlé G, Tojeiro R and Weaver BA (2024), Dec. The atomic gas sequence and mass-metallicity relation from dwarfs to massive galaxies. *MNRAS* 535 (3): 2341–2356. doi:10.1093/mnras/stae2477. 2408.03996.
- Segers MC, Schaye J, Bower RG, Crain RA, Schaller M and Theuns T (2016), Sep. The origin of the α -enhancement of massive galaxies. *MNRAS* 461 (1): L102–L106. doi:10.1093/mnras/slwl111. 1603.05653.
- Somerville RS and Davé R (2015), Aug. Physical Models of Galaxy Formation in a Cosmological Framework. *ARA&A* 53: 51–113. doi:10.1146/annurev-astro-082812-140951. 1412.2712.
- Spitoni E, Romano D, Matteucci F and Ciotti L (2015), Apr. The Effect of Stellar Migration on Galactic Chemical Evolution: A Heuristic Approach. *ApJ* 802 (2), 129. doi:10.1088/0004-637X/802/2/129. 1407.5797.
- Stanway ER and Eldridge JJ (2018), Sep. Re-evaluating old stellar populations. *MNRAS* 479 (1): 75–93. doi:10.1093/mnras/sty1353. 1805.08784.
- Stasińska G, Tenorio-Tagle G, Rodríguez M and Henney WJ (2007), Aug. Enrichment of the interstellar medium by metal-rich droplets and the abundance bias in H II regions. *A&A* 471 (1): 193–204. doi:10.1051/0004-6361:20065675. 0706.1225.
- Steidel CC, Strom AL, Pettini M, Rudie GC, Reddy NA and Trainor RF (2016), Aug. Reconciling the Stellar and Nebular Spectra of High-redshift Galaxies. *ApJ* 826: 159. doi:10.3847/0004-637X/826/2/159.
- Stott JP, Sobral D, Swinbank AM, Smail I, Bower R, Best PN, Sharples RM, Geach JE and Matthee J (2014), Sep. A relationship between specific star formation rate and metallicity gradient within $z = 1$ galaxies from KMOS-HIZELS. *MNRAS* 443: 2695–2704. doi:10.1093/mnras/stu1343.
- Strom AL, Steidel CC, Rudie GC, Trainor RF and Pettini M (2017a), Nov. Measuring the Physical Conditions in High-Redshift Star-Forming Galaxies: Insights from KBSS-MOSFIRE. *ArXiv e-prints*.
- Strom AL, Steidel CC, Rudie GC, Trainor RF, Pettini M and Reddy NA (2017b), Feb. Nebular Emission Line Ratios in $z = 2-3$ Star-forming Galaxies with KBSS-MOSFIRE: Exploring the Impact of Ionization, Excitation, and Nitrogen-to-Oxygen Ratio. *ApJ* 836: 164. doi:10.3847/1538-4357/836/2/164.
- Suresh J, Rubin KHR, Kannan R, Werk JK, Hernquist L and Vogelsberger M (2017), Mar. On the OVI abundance in the circumgalactic medium of low-redshift galaxies. *MNRAS* 465 (3): 2966–2982. doi:10.1093/mnras/stw2499. 1511.00687.
- Sánchez SF, Kennicutt RC, Gil de Paz A, van de Ven G, Vílchez JM, Wisotzki L, Walcher CJ, Mast D, Aguerri JAL, Albiol-Pérez S, Alonso-Herrero A, Alves J, Bakos J, Bartáková T, Bland-Hawthorn J, Boselli A, Bomans DJ, Castillo-Morales A, Cortijo-Ferrero C, de Lorenzo-Cáceres A, Del Olmo A, Dettmar RJ, Díaz A, Ellis S, Falcón-Barroso J, Flores H, Gallazzi A, García-Lorenzo B, González Delgado R, Gruel N, Haines T, Hao C, Husemann B, Iglésias-Páramo J, Jahnke K, Johnson B, Jungwiert B, Kalinova V, Kehrig C, Kupko D, López-Sánchez AR, Lyubenova M, Marino RA, Mármoel-Queraltó E, Márquez I, Masegosa J, Meidt S, Mendez-Abreu J, Monreal-Ibero A, Montijo C, Mourão AM, Palacios-

- Navarro G, Papaderos P, Pasquali A, Peletier R, Pérez E, Pérez I, Quirrenbach A, Relaño M, Rosales-Ortega FF, Roth MM, Ruiz-Lara T, Sánchez-Blázquez P, Sengupta C, Singh R, Stanishev V, Trager SC, Vazdekis A, Viironen K, Wild V, Zibetti S and Ziegler B (2012), Feb. CALIFA, the Calar Alto Legacy Integral Field Area survey. I. Survey presentation. *A&A* 538: A8. doi:10.1051/0004-6361/201117353.
- Sánchez SF, Rosales-Ortega FF, Iglesias-Páramo J, Mollá M, Barrera-Ballesteros J, Marino RA, Pérez E, Sánchez-Blázquez P, González Delgado R, Cid Fernandes R, de Lorenzo-Cáceres A, Mendez-Abreu J, Galbany L, Falcon-Barroso J, Miralles-Caballero D, Husemann B, García-Benito R, Mast D, Walcher CJ, Gil de Paz A, García-Lorenzo B, Jungwiert B, Vilchez JM, Jilková L, Lyubenova M, Cortijo-Ferrero C, Díaz AI, Wisotzki L, Márquez I, Bland-Hawthorn J, Ellis S, van de Ven G, Jahnke K, Papaderos P, Gomes JM, Mendoza MA and López-Sánchez AR (2014), Mar. A characteristic oxygen abundance gradient in galaxy disks unveiled with CALIFA. *A&A* 563: A49. doi:10.1051/0004-6361/201322343.
- Sánchez SF, García-Benito R, Zibetti S, Walcher CJ, Husemann B, Mendoza MA, Galbany L, Falcón-Barroso J, Mast D, Aceituno J, Aguerri JAL, Alves J, Amorim AL, Ascasibar Y, Barrado-Navascues D, Barrera-Ballesteros J, Bekeraite S, Bland-Hawthorn J, Cano Díaz M, Cid Fernandes R, Cavichia O, Cortijo C, Dannerbauer H, Demleitner M, Díaz A, Dettmar RJ, de Lorenzo-Cáceres A, del Olmo A, Galazzi A, García-Lorenzo B, Gil de Paz A, González Delgado R, Holmes L, Iglesias-Páramo J, Kehrig C, Kelz A, Kennicutt RC, Kleemann B, Lacerda EAD, López Fernández R, López Sánchez AR, Lyubenova M, Marino R, Márquez I, Mendez-Abreu J, Mollá M, Monreal-Ibero A, Ortega Minakata R, Torres-Papaqui JP, Pérez E, Rosales-Ortega FF, Roth MM, Sánchez-Blázquez P, Schilling U, Spekkens K, Vale Asari N, van den Bosch RCE, van de Ven G, Vilchez JM, Wild V, Wisotzki L, Yıldırım A and Ziegler B (2016), Oct. CALIFA, the Calar Alto Legacy Integral Field Area survey. IV. Third public data release. *A&A* 594: A36. doi:10.1051/0004-6361/201628661.
- Sánchez-Menguiano L, Sánchez SF, Pérez I, Debattista VP, Ruiz-Lara T, Florido E, Cavichia O, Galbany L, Marino RA, Mast D, Sánchez-Blázquez P, Méndez-Abreu J, de Lorenzo-Cáceres A, Catalán-Torrecilla C, Cano-Díaz M, Márquez I, McIntosh DH, Ascasibar Y, García-Benito R, González Delgado RM, Kehrig C, López-Sánchez AR, Mollá M, Bland-Hawthorn J, Walcher CJ and Costantin L (2017), Jul. Arm and interarm abundance gradients in CALIFA spiral galaxies. *A&A* 603: A113. doi:10.1051/0004-6361/201630062.
- Sánchez-Menguiano L, Sánchez SF, Pérez I, Ruiz-Lara T, Galbany L, Anderson JP, Krühler T, Kunarayakti H and Lyman JD (2018), Feb. The shape of oxygen abundance profiles explored with MUSE: evidence for widespread deviations from single gradients. *A&A* 609: A119. doi:10.1051/0004-6361/201731486.
- Tacconi LJ, Genzel R, Saintonge A, Combes F, García-Burillo S, Neri R, Bolatto A, Contini T, Förster Schreiber NM, Lilly S, Lutz D, Wuyts S, Accurso G, Boissier J, Boone F, Bouché N, Bournaud F, Burkert A, Carollo M, Cooper M, Cox P, Feruglio C, Freundlich J, Herrera-Camus R, Juneau S, Lippa M, Naab T, Renzini A, Salome P, Sternberg A, Tadaki K, Übler H, Walter F, Weiner B and Weiss A (2018), Feb. PHIBSS: Unified Scaling Relations of Gas Depletion Time and Molecular Gas Fractions. *ApJ* 853: 179. doi:10.3847/1538-4357/aaa4b4.
- Tacconi LJ, Genzel R and Sternberg A (2020), Aug. The Evolution of the Star-Forming Interstellar Medium Across Cosmic Time. *ARA&A* 58: 157–203. doi:10.1146/annurev-astro-082812-141034. 2003.06245.
- Telford OG, Dalcanton JJ, Skillman ED and Conroy C (2016), Aug. Exploring Systematic Effects in the Relation Between Stellar Mass, Gas Phase Metallicity, and Star Formation Rate. *ApJ* 827: 35. doi:10.3847/0004-637X/827/1/35.
- Tominaga N, Umeda H and Nomoto K (2007), May. Supernova Nucleosynthesis in Population III 13–50 M_{Solar} Stars and Abundance Patterns of Extremely Metal-poor Stars. *ApJ* 660 (1): 516–540. doi:10.1086/513063. astro-ph/0701381.
- Topping MW, Shapley AE, Sanders RL, Kriek M, Reddy NA, Coil AL, Mobasher B, Siana B, Freeman WR, Shvaei I, Azadi M, Price SH, Leung GCK, Fetherolf T, de Groot L, Zick T, Fornasini FM, Barro G and Runco JN (2021), Sep. The MOSDEF survey: the mass-metallicity relationship and the existence of the FMR at $z \approx 1.5$. *MNRAS* 506 (1): 1237–1249. doi:10.1093/mnras/stab1793. 2103.09245.
- Topping MW, Stark DP, Senchyna P, Plat A, Zitrin A, Endsley R, Charlot S, Furtak LJ, Maseda MV, Smit R, Mainali R, Chevallard J, Molyneux S and Rigby JR (2024), Apr. Metal-poor star formation at $z \approx 6$ with JWST: new insight into hard radiation fields and nitrogen enrichment on 20 pc scales. *MNRAS* 529 (4): 3301–3322. doi:10.1093/mnras/stae682. 2401.08764.
- Toribio San Cipriano L, Domínguez-Guzmán G, Esteban C, García-Rojas J, Mesa-Delgado A, Bresolin F, Rodríguez M and Simón-Díaz S (2017), May. Carbon and oxygen in H II regions of the Magellanic Clouds: abundance discrepancy and chemical evolution. *MNRAS* 467 (3): 3759–3774. doi:10.1093/mnras/stx328. 1702.01120.
- Torrey P, Vogelsberger M, Marinacci F, Pakmor R, Springel V, Nelson D, Naiman J, Pillepich A, Genel S, Weinberger R and Hernquist L (2019), Apr. The evolution of the mass-metallicity relation and its scatter in IllustrisTNG. *MNRAS* 484 (4): 5587–5607. doi:10.1093/mnras/stz243. 1711.05261.
- Tremonti CA, Heckman TM, Kauffmann G, Brinchmann J, Charlot S, White SDM, Seibert M, Peng EW, Schlegel DJ, Uomoto A, Fukugita M and Brinkmann J (2004), Oct. The Origin of the Mass-Metallicity Relation: Insights from 53,000 Star-forming Galaxies in the Sloan Digital Sky Survey. *ApJ* 613: 898–913. doi:10.1086/423264.
- Trussler J, Maiolino R, Maraston C, Peng Y, Thomas D, Goddard D and Lian J (2020), Feb. Both starvation and outflows drive galaxy quenching. *MNRAS* 491 (4): 5406–5434. doi:10.1093/mnras/stz3286. 1811.09283.
- Tsamis YG, Barlow MJ, Liu XW, Danziger IJ and Storey PJ (2003), Jan. Heavy elements in Galactic and Magellanic Cloud HII regions: recombination-line versus forbidden-line abundances. *MNRAS* 338 (3): 687–710. doi:10.1046/j.1365-8711.2003.06081.x. astro-ph/0209534.
- Tumlinson J, Thom C, Werk JK, Prochaska JX, Tripp TM, Weinberg DH, Peebles MS, O’Meara JM, Oppenheimer BD, Meiring JD, Katz NS, Davé R, Ford AB and Sembach KR (2011), Nov. The Large, Oxygen-Rich Halos of Star-Forming Galaxies Are a Major Reservoir of Galactic Metals. *Science* 334 (6058): 948. doi:10.1126/science.1209840. 1111.3980.
- Tumlinson J, Peebles MS and Werk JK (2017), Aug. The Circumgalactic Medium. *ARA&A* 55 (1): 389–432. doi:10.1146/annurev-astro-091916-055240. 1709.09180.
- Ucci G, Dayal P, Hutter A, Kobayashi C, Gottlöber S, Yepes G, Hunt L, Legrand L and Tortora C (2023), Jan. Astraeus V: the emergence and evolution of metallicity scaling relations during the epoch of reionization. *MNRAS* 518 (3): 3557–3575. doi:10.1093/mnras/stac2654. 2112.02115.
- Vanni I, Salvadori S, Skúladóttir Á, Rossi M and Koutsouridou I (2023), Dec. Characterizing the true descendants of the first stars. *MNRAS* 526 (2): 2620–2644. doi:10.1093/mnras/stad2910. 2309.07958.
- Vanzella E, De Barros S, Cupani G, Karman W, Gronke M, Balestra I, Coe D, Mignoli M, Brusa M, Calura F, Caminha GB, Caputi K, Castellano M, Christensen L, Comastri A, Cristiani S, Dijkstra M, Fontana A, Giallongo E, Giavalisco M, Gilli R, Grazian A, Grillo C, Koekemoer A, Meneghetti M, Nonino M, Pentericci L, Rosati P, Schaerer D, Verhamme A, Vignali C and Zamorani G (2016), Apr. High-resolution Spectroscopy of a Young, Low-metallicity Optically Thin $L = 0.02L^*$ Star-forming Galaxy at $z = 3.12$. *ApJ* 821 (2), L27. doi:10.3847/2041-8205/821/2/L27. 1603.01616.
- Venditti A, Bromm V, Finkelstein SL, Graziani L and Schneider R (2024), Jan. The first fireworks: A roadmap to Population III stars during the epoch of reionization through pair-instability supernovae. *MNRAS* 527 (3): 5102–5116. doi:10.1093/mnras/stad3513. 2306.06501.
- Vincenzo F, Belfiore F, Maiolino R, Matteucci F and Ventura P (2016a), Mar. Nitrogen and oxygen abundances in the Local Universe. *MNRAS* doi:10.1093/mnras/stw532.
- Vincenzo F, Matteucci F, Belfiore F and Maiolino R (2016b), Feb. Modern yields per stellar generation: the effect of the IMF. *MNRAS* 455: 4183–4190. doi:10.1093/mnras/stv2598.

- Vink JS (2024), Oct. Very massive stars and Nitrogen-emitting galaxies. *arXiv e-prints*, arXiv:2410.18980doi:10.48550/arXiv.2410.18980. 2410.18980.
- Vogelsberger M, Genel S, Springel V, Torrey P, Sijacki D, Xu D, Snyder G, Nelson D and Hernquist L (2014), Oct. Introducing the Illustris Project: simulating the coevolution of dark and visible matter in the Universe. *MNRAS* 444 (2): 1518–1547. doi:10.1093/mnras/stu1536. 1405.2921.
- Wang X, Jones TA, Treu T, Morishita T, Abramson LE, Brammer GB, Huang KH, Malkan MA, Schmidt KB, Fontana A, Grillo C, Henry AL, Karman W, Kelly PL, Mason CA, Mercurio A, Rosati P, Sharon K, Trenti M and Vulcani B (2017), Mar. The Grism Lens-amplified Survey from Space (GLASS). X. Sub-kiloparsec Resolution Gas-phase Metallicity Maps at Cosmic Noon behind the Hubble Frontier Fields Cluster MACS1149.6+2223. *ApJ* 837: 89. doi:10.3847/1538-4357/aa603c.
- Wang X, Jones TA, Treu T, Hirtenstein J, Brammer GB, Daddi E, Meng XL, Morishita T, Abramson LE, Henry AL, Peng YJ, Schmidt KB, Sharon K, Trenti M and Vulcani B (2019), Sep. Discovery of Strongly Inverted Metallicity Gradients in Dwarf Galaxies at $z \sim 2$. *ApJ* 882: 94. doi:10.3847/1538-4357/ab3861.
- Watanabe K, Ouchi M, Nakajima K, Isose Y, Tominaga N, Suzuki A, Ishigaki MN, Nomoto K, Takahashi K, Harikane Y, Hatano S, Kusakabe H, Moriya TJ, Nishigaki M, Ono Y, Onodera M and Sugahara Y (2024), Feb. EMPRESS. XIII. Chemical Enrichment of Young Galaxies Near and Far at $z \sim 0$ and $4-10$: Fe/O, Ar/O, S/O, and N/O Measurements with a Comparison of Chemical Evolution Models. *ApJ* 962 (1), 50. doi:10.3847/1538-4357/ad13ff. 2305.02078.
- Witstok J, Shivaeei I, Smit R, Maiolino R, Carniani S, Curtis-Lake E, Ferruit P, Arribas S, Bunker AJ, Cameron AJ, Charlot S, Chevillard J, Curti M, de Graaff A, D'Eugenio F, Giardino G, Looser TJ, Rawle T, Rodríguez del Pino B, Willott C, Alberts S, Baker WM, Boyett K, Egami E, Eisenstein DJ, Endsley R, Hainline KN, Ji Z, Johnson BD, Kumari N, Lyu J, Nelson E, Perna M, Rieke M, Robertson BE, Sandles L, Saxena A, Scholtz J, Sun F, Tacchella S, Williams CC and Willmer CNA (2023), Sep. Carbonaceous dust grains seen in the first billion years of cosmic time. *Nature* 621 (7978): 267–270. doi:10.1038/s41586-023-06413-w. 2302.05468.
- Worthey G, Faber SM, Gonzalez JJ and Burstein D (1994), Oct. Old Stellar Populations. V. Absorption Feature Indices for the Complete Lick/IDS Sample of Stars. *ApJS* 94: 687. doi:10.1086/192087.
- Wuyts E, Wisnioski E, Fossati M, Förster Schreiber NM, Genzel R, Davies R, Mendel JT, Naab T, Röttgers B, Wilman DJ, Wuyts S, Bandara K, Beifiori A, Belli S, Bender R, Brammer GB, Burkert A, Chan J, Galametz A, Kulkarni SK, Lang P, Lutz D, Momcheva IG, Nelson EJ, Rosario D, Saglia RP, Seitz S, Tacconi LJ, Tadaki Ki, Übler H and van Dokkum P (2016), Aug. The Evolution of Metallicity and Metallicity Gradients from $z = 2.7$ to 0.6 with KMOS³⁴⁵. *ApJ* 827: 74. doi:10.3847/0004-637X/827/1/74.
- Yates RM, Kauffmann G and Guo Q (2012), May. The relation between metallicity, stellar mass and star formation in galaxies: an analysis of observational and model data. *MNRAS* 422: 215–231. doi:10.1111/j.1365-2966.2012.20595.x.
- Yates RM, Schady P, Chen TW, Schweyter T and Wiseman P (2020), Feb. Present-day mass-metallicity relation for galaxies using a new electron temperature method. *A&A* 634, A107. doi:10.1051/0004-6361/201936506. 1901.02890.
- Yates RM, Péroux C and Nelson D (2021), Dec. Cosmic metal density evolution in neutral gas: insights from observations and cosmological simulations. *MNRAS* 508 (3): 3535–3550. doi:10.1093/mnras/stab2837. 2109.06888.
- York DG, Adelman J, Anderson Jr. JE, Anderson SF, Annis J, Bahcall NA, Bakken JA, Barkhouser R, Bastian S, Berman E, Boroski WN, Bracker S, Briegel C, Briggs JW, Brinkmann J, Brunner R, Burles S, Carey L, Carr MA, Castander FJ, Chen B, Colestock PL, Connolly AJ, Crocker JH, Csabai I, Czarapata PC, Davis JE, Doi M, Dombeck T, Eisenstein D, Ellman N, Elms BR, Evans ML, Fan X, Federwitz GR, Fiscelli L, Friedman S, Frieman JA, Fukugita M, Gillespie B, Gunn JE, Gurubani VK, de Haas E, Haldeman M, Harris FH, Hayes J, Heckman TM, Hennessy GS, Hindsley RB, Holm S, Holmgren DJ, Huang Ch, Hull C, Husby D, Ichikawa SI, Ichikawa T, Ivezić Z, Kent S, Kim RJS, Kinney E, Klaene M, Kleinman AN, Kleinman S, Knapp GR, Korienek J, Kron RG, Kunszt PZ, Lamb DQ, Lee B, Leger RF, Limmongkol S, Lindenmeyer C, Long DC, Loomis C, Loveday J, Lucinio R, Lupton RH, MacKinnon B, Mannery EJ, Mantsch PM, Margon B, McGehee P, McKay TA, Meiksin A, Merelli A, Monet DG, Munn JA, Narayanan VK, Nash T, Neilsen E, Neswold R, Newberg HJ, Nichol RC, Nicinski T, Nonino M, Okada N, Okamura S, Ostriker JP, Owen R, Pauls AG, Peoples J, Peterson RL, Petravick D, Pier JR, Pope A, Pordes R, Prosapio A, Rechenmacher R, Quinn TR, Richards GT, Richmond MW, Rivetta CH, Rockosi CM, Ruthmansdorfer K, Sandford D, Schlegel DJ, Schneider DP, Sekiguchi M, Sergey G, Shimasaku K, Siegmund WA, Smee S, Smith JA, Snedden S, Stone R, Stoughton C, Strauss MA, Stubbs C, SubbaRao M, Szalay AS, Szapudi I, Szokoly GP, Thakur AR, Tremonti C, Tucker DL, Uomoto A, Vanden Berk D, Vogeley MS, Waddell P, Wang Si, Watanabe M, Weinberg DH, Yanny B, Yasuda N and SDSS Collaboration (2000), Sep. The Sloan Digital Sky Survey: Technical Summary. *AJ* 120: 1579–1587. doi:10.1086/301513.
- Yuan TT, Kewley LJ and Rich J (2013), Apr. Systematics in Metallicity Gradient Measurements. I. Angular Resolution, Signal to Noise, and Annular Binning. *ApJ* 767: 106. doi:10.1088/0004-637X/767/2/106.
- Zahid HJ, Dima GI, Kudritzki RP, Kewley LJ, Geller MJ, Hwang HS, Silverman JD and Kashino D (2014), Aug. The Universal Relation of Galactic Chemical Evolution: The Origin of the Mass-Metallicity Relation. *ApJ* 791: 130. doi:10.1088/0004-637X/791/2/130.
- Zahid HJ, Kudritzki RP, Conroy C, Andrews B and Ho IT (2017), Sep. Stellar Absorption Line Analysis of Local Star-forming Galaxies: The Relation between Stellar Mass, Metallicity, Dust Attenuation, and Star Formation Rate. *ApJ* 847: 18. doi:10.3847/1538-4357/aa88ae.